Experimental Study of Spin-Up of a Fluid-Filled Cylindrical Tank

Jakob Svensson

A thesis presented for the degree of
Master of Mechanical Engineering

LUND UNIVERSITY

Energy Sciences
Lund Technical University
Sweden
2018-02-22

This degree project for the degree of Master of Science in Engineering has been conducted at the Division of Fluid Mechanics , Department of Energy Sciences, Faculty of Engineering,
Lund University, and at European Space Research and Technology Centre (ESTEC), The Netherlands.

Supervisor at the Division of Fluid Mechanics was Professor Johan Revstedt.
Supervisor at ESTEC was Richard Schwane.
Examiner at Lund University was Professor Xue-Song Bai.
The project was carried out in cooperation with Master's Student in Engineering Physics; Dennis Kröger.

Thesis for the Degree of Master of Science in Engineering
ISRN LUTMDN/TMHP-18/5405-SE
ISSN 0282-1990

Fluid Mechanics
Department of Energy Sciences
Faculty of Engineering, Lund University
Box 118, 221 00 Lund
Sweden
www.energy.lth.se

Abstract

To ensure safety on upper stage rockets, the fluid dynamic phenomenon known as sloshing in the liquid propellant tanks needs to be understood. CFD is a relatively cheap tool, but studies by Schmitt [7] suggest that models currently used for simulations do not predict the flow behavior. To verify computational models, experiments are setup on a cylindrical tank. The time for the fluid to become steady in a cylindrical tank rotating along the axis is measured for both a completely water filled tank and a tank half-filled with water and half-filled with air. The method for measuring the time until steady state uses an open-source image-analysis tool based on Particle Image Velocimetry. The results for the air-water tank show no dependency on rotational speed or geometry of the tank. The results for the completely filled tank show spin-up times coherent with theoretical data for laminar Ekman layer boundary flow predicted by Sedney and Gerber [8] and show that the spin-up time is given by $E_s = \frac{8}{\sqrt{\nu}\sqrt{\Omega}}$.

Acknowledgements

This project has been carried out at the European Space Research and Technology Centre in Noordwijk, the Netherlands. I would like to thank Dennis Kröger, with whom I have been sharing an office and ideas with during the whole project. Most of the ideas in this report would not be possible without the discussions we had.

I also like to thank Henrike Jakob, who did the preperatory work for this project, like programming and building a Wi-Fi controlled electrolysis machine. I would like to thank Ronan Flanagan who helped set up the experimental tank and did important work on the simulations of the flow case. I would like to thank Johan Steelant and Csaba Jeger who helped me understand the fluid dynamics of bubbles suspended in water. I would like to thank Dominic Doyle who helped me with the optics.

Special thanks to Richard Schwane who made this project possible and for giving me this opportunity. He never stopped having ideas on how to make this project better and were always up for a discussion on my results.

Jakob Svensson, 2018, Noordwijk.

Contents

List of Figures

List of Tables

Abbreviations

BANNER Larger tank

CFD Computational Fluid Dynamics

ESA European Space Agency

LANG Smaller tank

PIV Particle Image Velocimetry

PIV* (Read "PIV-Star") Modified Particle Image Velocimetry technique

List of symbols

Variable	Description
δ	Ekman boundary layer thickness
γ	Surface Tension (N/m)
ν	Kinematic Viscosity (m^2/s)
Ω	Rotational speed (rad/s)
ρ	Density (kg/m^3)
σ	Standard deviation
τ	Response time
θ	Azimuthal coordinate (rad)
A	Area (m^2)
a_l	acceleration (linear) (m/s^2)
a_r	acceleration (rotational) ($degrees/s^2$)
c	Half-height of cylinder (m)
C	Constant
c_d	Drag coefficient
D	Diameter (m)
E	Spin-up time
Ek	Ekman number
F	Force (N)
g	Gravitational Constant (m/s^2)
h	Height (m)
I	Moment of Inertia (kgm^2)
M	Moment (Nm)
m	Mass (kg)
P	Pressure (N/m^2)
r	Radius, radial coordinate (m)
Re	Reynolds number
Ro	Rossby number
t	time (s)
U	Radial or General flow velocity (m/s)
V	Azimuthal flow velocity (m/s)
V	Volume (m^3)
W	Vertical flow Velocity (m/s)
z	Vertical coordinate (m)

Reading the Report

The first section is written to give the reader an understanding of the problem and describe what experiments are conducted in this report. The second section is a description of video results so the reader can see the raw results that were analyzed in this report. The third section handles the theory behind the methods used in this project. The fourth section describes the methods used in this report. The fifth section describes the experimental setup. The sixth section discusses and presents the results of the report. The seventh section draws conclusions of the results. The eight section discusses further work. Most of the results are presented in the appendix, and the sixth section only presents the summarized results that is most interesting for the reader.

1 Introduction

1.1 Motivation

To safely and accurately maneuver any satellites or upper stage rockets, the dynamics of the sloshing of fuel in the said vehicles needs to be understood. The specific motivation for this project has been to gain understanding of the sloshing dynamics in the Vinci engines on the Ariane 6 rocket developed by ESA. The problem using in-situ experiments would be that they are relatively expensive and time consuming. The sloshing dynamics need to be simulated using CFD to save resources. The CFD will be verified with smaller-scale experiments.[1][2]

1.2 Background

ESA is a intergovernmental organization with 22 member states and has as an objective to do research and development in space exploration. The mission of ESA is to develop Europe's space capability and to make sure that the governmental investment in space continues to deliver benefits to the citizens of Europe and the world. ESTEC is the European Space Research and Technology Centre and is located in Noordwijk in the Netherlands. Most of the research and testing at ESA projects is done at ESTEC. The tests for this thesis were done in the propulsion laboratory at ESTEC. [3]

The Ariane 6 rocket is being developed by ESA and is planned to have its first launch in the year 2020. The Ariane 6 project is being developed to maintain Europe's leadership in a fast-changing commercial launch-service. The Ariane 6 rocket will differ in many ways to Ariane 5 rocket, one being the restartability of the upper stage. This will allow multiple payloads, which will increase the competitiveness relative to other launchers.[4] The different payloads have individual demands for the spin-rate at the release from the rocket, which will require the upper stage to perform spin-up and spin-down maneuvers. It is important to predict the behavior and movement of the liquid propellant during maneuvers, since a ingestion of gas bubbles or similar interruptions of the continuous flow of propellant to the engine will lead to catastrophic failure. [1]

The engine for the upper stage of the Ariane 6 rocket will be a Vinci engine providing 180 kN of thrust and with capability of multiple restarts. The propellant will be liquid hydrogen and liquid oxygen. [5]

During the spin-maneuvers the liquid propellant could be subjected to a phenomenon called "sloshing". The definition of sloshing is the motion of a free liquid surface inside a container. It is caused by any disturbance to the partially filled container. The phenomenon of sloshing can cause several different types of behaviors of the liquid interacting with the elastic material of the tank. The phenomenon is also affected by the low-gravity environment and the cryogenics of the liquid hydrogen. The phenomenon focused on for the Ariane 6 is the difference in pressure distribution due to sloshing causing the liquid hydrogen to boil and creating gas bubbles which would destroy the engine.[6]

To reliably perform the required maneuvers for the upper stage the liquid propellant needs to be simulated using CFD. CFD modeling is faster and cheaper than performing actual experiments in space and is crucial for the understanding of the sloshing behavior of the fluid. As suggested by Schmitt [7], using commercial software to predict the contact angles and pressure distributions in a

cryogenic, low-gravity environment is not coherent with experimental findings. This would require an update of the models to make sure that the results from simulations give the same results as experimental data. [7]

To simplify the flow setup for the simulations only the rotating cylinder was considered. A rotating cylinder containing water was simulated by Jakob [1]. The cylinder was simulated being filled with 100% and being filled with 50%. There was also effort made to verify these simulations with experimental data acquired at the propulsion lab at ESTEC. The experiments are updated and re-evaluated in this report. [1]

1.3 Purpose of Work

The experiments are influenced by the work of Jakob [1] and builds on the work she started. Several methods were considered and tested and the methods generating reliable results are presented in this report. Two different tanks were used in the experiments, one being the same as used by Jakob [1] and one specially produced for these experiments with improved quality. The tank used Jakob [1] is said to have a significant wobble, deeming the results unreliable for comparison with CFD.

The experiments in this report are made to support simulation with verification data. The emphasis of the report will be the spin-up and the time it takes for the tank to reach steady state. Two types of experiments was conducted, one type on half-filled tank and one for fully filled tank. The medium will be water and air if the tank is not fully filled.

1.4 Naming the tanks

Two separate tanks were used for the experiments. One smaller tank, used by Jakob [1] with the radius of 96 mm and a height of 257 mm. The tank is named LANG after the alter-ego of "Antman" from the Marvel Comics. The other tank, which most of the experiments in this report are based on, is named BANNER, since it is bigger and Banner is the alter-ego of the Incredible Hulk from the Marvel comics. The measurements of BANNER is a radius of 0.15 m and a height of $0.2m$. If the experiments continue, the following tanks could be named after more characters from the Marvel Universe.

LANG and BANNER were either Fully-filled or Half-filled with water. The flow field is different for the amount of water in the tanks.

1.5 Videos

There were several videos created as a results of the experiments and can be found as an appendix under videos.

2 Theory

2.1 Steady State behavior

The second law of thermodynamics states that the entropy of any system must increase over time. This means the amount of usable energy decreases over time. It is therefore argued that the fluid in a rotating cylinder will reach solid-body rotation after some time, since in the frame of reference of the cylinder, solid-body rotation is the lowest amount of energy the system can have. The usable energy will dissipate through viscosity and in the end only the solid body rotation will remain, given that no energy is added to the system. For the experiments conducted in this report, the cylinder is not entirely isolated from the surroundings and the flow is disturbed by several factors. Solid-body rotation is indicated by a linear velocity profile in radial direction, which will be used as a reference in this report.

The mathematical prof of the steady state velocity profile can be found in the energy equation for polar coordinates using the viscous dissipation give by:

$$\Phi = 2\mu\left[\left(\frac{\partial u_r}{\partial r}\right)^2 + \left(\frac{1}{r}\frac{\partial u_\theta}{\partial \theta} + \frac{u_r}{r}\right)^2 + \left(\frac{\partial u_z}{\partial z}\right)^2\right] + \mu\left[\left(\frac{1}{r}\frac{\partial u_r}{\partial \theta} + \frac{\partial u_\theta}{\partial r} - \frac{u_\theta}{r}\right)^2 + \left(\frac{\partial u_\theta}{\partial z} + \frac{1}{r}\frac{\partial u_z}{\partial \theta}\right)^2 + \left(\frac{\partial u_z}{\partial r} + \frac{\partial u_r}{\partial z}\right)^2\right] - \frac{2}{3}\mu\left(\frac{1}{r}\frac{\partial (r u_r)}{\partial r} + \frac{1}{r}\frac{\partial u_\theta}{\partial \theta} + \frac{\partial u_z}{\partial z}\right)^2$$

*

Where the only non-zero components are given by:

$$\frac{\partial u_\theta}{\partial r} = \frac{u_\theta}{r} = \Omega \tag{1}$$

Which gives a viscous dissipation equal to zero at solid body rotation.

When the flow reaches near-Solid-Body rotation the fluid is said to be in steady state. When there are still transient movement in the tank, the flow is said to be unsteady. When examining flow with an open air-water interface, the steady state sometimes reference to a constant pressure gradient, indicated in the text.

2.2 Coordinate system and velocities

A coordinate system is implemented for a cylindrical tank, where the cylindrical spacial coordinates are given by (r, θ, z) shown in figure 1 and the velocities (U, V, W) seen in figure 2.

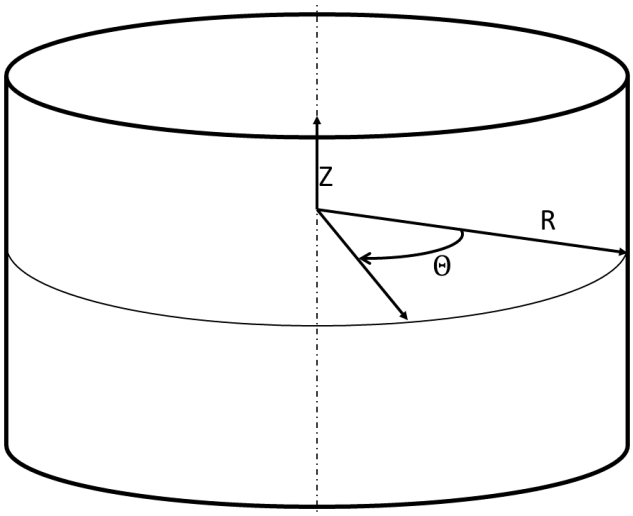

Figure 1: The coordinates in the cylindrical tank

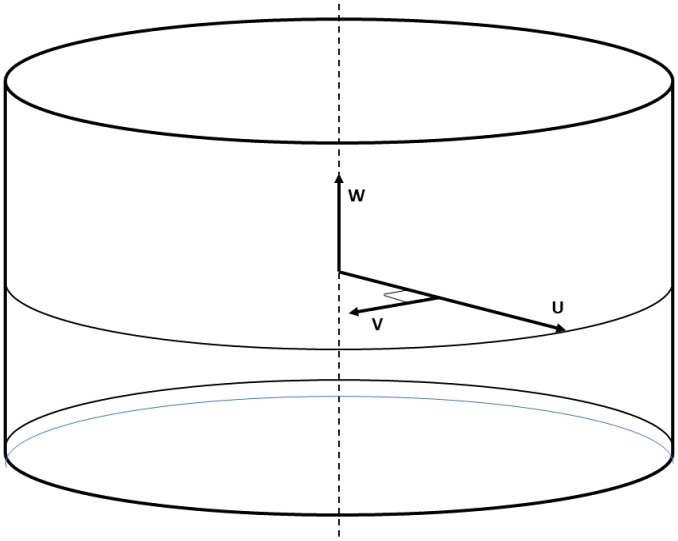

Figure 2: Orientation of velocities

2.3 Steady state in an half-filled tank

In solid-body rotation the pressure gradient is balanced with the centripetal force:

$$\frac{1}{\rho}\frac{dP}{dr} = \Omega^2 r \tag{2}$$

Where ρ is the density of the fluid, P is the pressure, r is radius and Ω is the angular speed. This equation integrated gives the pressure distribution of:

$$P = \rho\frac{\Omega^2 r^2}{2} + P_0 \rightarrow h(r) = \frac{\Omega^2 r^2}{2g} + h_0 \tag{3}$$

The equation to the right side represents the pressure distribution as a hydraulic height. g is the gravitational constant and h_0 is the lowest point of the parabola. The volume of the fluid at rest is given by:

$$V = h_{rest} * A = h_{rest} * r^2 * \pi \tag{4}$$

The volume of the fluid in motion is given by the solid of revolution of the parabola added to the volume of the lowest point of the parabola multiplied with the bottom area of the cylinder. The solid of revolution is found by:

$$V_{top} = h_{max} * A - \int_{h_{min}}^{h_{max}} r(h)^2 \pi dh \tag{5}$$

Where h_{min} is the lowest point of the parabola and h_{max} is the highest point of the parabola. $r(h)$ is found by rearranging the equation for hydraulic height. This gives:

$$V_{top} = h_{max} r^2 \pi - \frac{\pi g h^2}{\Omega^2} = \frac{\Omega^2 r^4 \pi}{2g} - \frac{\Omega^2 r^4 \pi}{4g} = \frac{\Omega^2 r^4 \pi}{4g} \tag{6}$$

Where V_{top} is the volume of the part of fluid shaped like a parabola. The lowest part of the parabola is found through:

$$h_{rest} * A = h_0 * A + V_{top} \rightarrow h_0 = h_{rest} - V_{top}/A \tag{7}$$

The highest point of the parabola is found through the hydraulic height:

$$h_{max} = h_0 + \frac{\Omega^2 r_{tank}^2}{2g} \tag{8}$$

It is also noted that second term on the right-hand side in equation 8 can be seen as the total parabola height. This is defined as h_{tot}, which is more convenient to compare to numerical data.

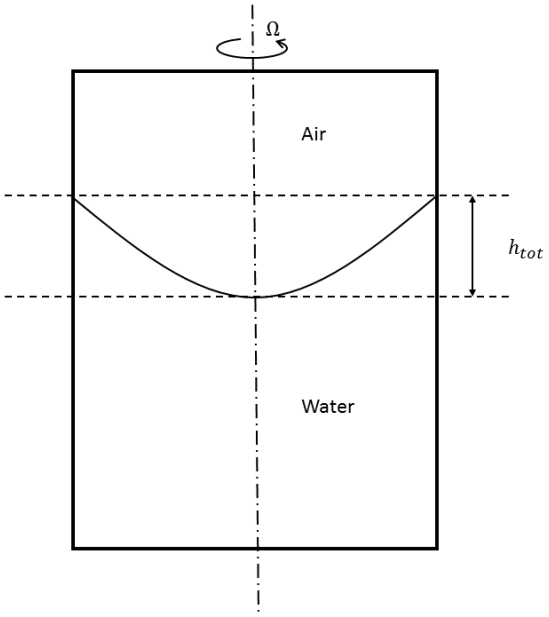

Figure 3: The shape of a parabola in a tank filled with water

$$h_{tot} = \frac{\Omega^2 r_{tank}^2}{2g} \tag{9}$$

The parabola height is an indication that Solid-Body rotation is reached, but is not an absolute measure on how close the system is to steady state. The steady state is defined by radial velocity profile, the pressure gradient is only a indication on steady state flow.

At the open surface the water and air will form a shear layer. This layer will be unstable due to Kelvin-Helmholtz instability. The instability is dampened by the surface tension of the water. The instabilities arise according to:[12]

$$|(U_1^2 - U_2^2)| < \frac{2(\rho_1 + \rho_2)}{\rho_1 \rho_2} \sqrt{[\gamma g(\rho_2 - \rho_1)]} \tag{10}$$

Where the notation of 1 indicates the properties of water and notation of 2 indicates properties of air. The shear layer will always have some wave formation due to the difference in velocity, but the instabilities will not propagate below this velocity difference.

The height of the parabola will be analyzed using image-analysis. When the parabola is fully developed the fluid is said to be in steady state, using the pressure in the tank as a reference. This is different from using the velocity as a measurement, since to measure steady state for the pressure the height of the parabola has to be measured with high accuracy. This is rather difficult since only image analysis tools are available.

As BANNER is made up of clear acrylic, and the water has different refractive index than air, the image will be skewed. Since the measurements require high accuracy to find the exact spin-up time, the actual measured parabola height will not be considered. Instead, the signal of the lowest point of the parabola will continuously be plotted as a function of time. This function will be smoothed using "Loess" smoothing to eliminate the noise created by the measuring method. "Loess" smoothing uses weighted linear least squares method and second degree polynomial model. The smoothed function is then differentiated and where the differentiated function reaches zero, steady state is said to be reached.

$$\frac{dh_{loess}}{dt} = 0 \tag{11}$$

2.4 Steady State in a Filled Tank

As the tank starts to rotate, an Ekman layer is formed. The physics behind the Ekman layer is that the centripetal force is not balanced with the pressure gradient in the boundary layer on the top and bottom walls. The fluid accelerates faster at the top and bottom walls since the core of flow in the tank will accelerate as momentum is transferred via viscosity to inner parts of the tank. The unbalanced forces result in a secondary flow structure shown in figure 4. This phenomenon is called Ekman pumping. A second type of boundary layer is formed on the vertical walls called Stewartson layer.[2]

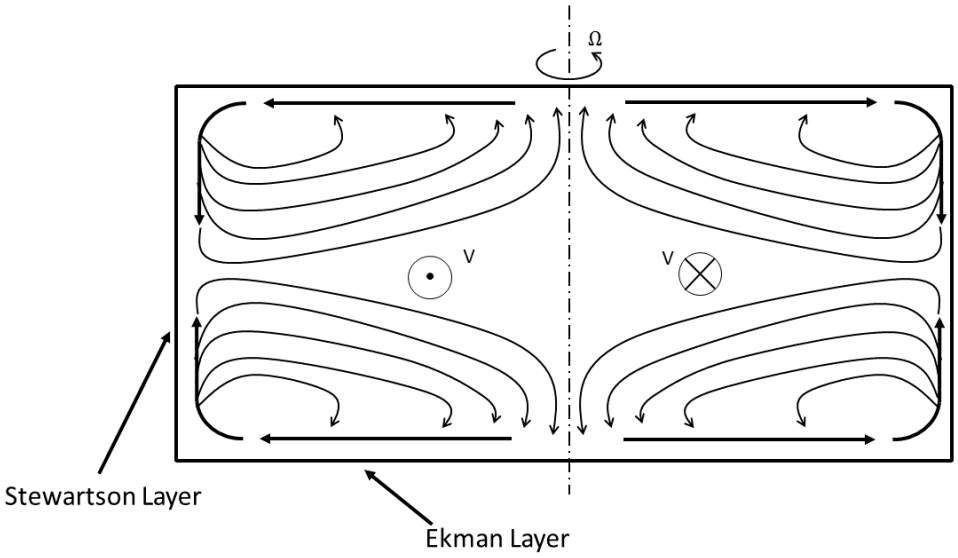

Figure 4: The primary flow (V) and the secondary flow (arrows) as the tank is spun up

To quantify the flow several dimensionless numbers are used. The Reynolds number is defined as:

$$Re = \frac{r^2\Omega}{\nu} \tag{12}$$

The Reynolds number is a dimensionless quantity defined as the ratio between the inertial forces and the viscous forces. The Reynolds number is used to determine if a flow is laminar or turbulent.

The second number used is the Ekman number, defined as [8]:

$$Ek = \frac{\nu}{\Omega c^2} \tag{13}$$

The Ekman number is the ratio of viscous forces to Coriolis force. It should be noted that some studies use another definition of the Ekman number, given by [9]:

$$Ek = \frac{\nu}{r^2 * \Omega} = Re^{-1} \tag{14}$$

This definition is not used in this report since it does not provide any information of the flow that the Reynolds number has not already given.

The Ekman boundary thickness is given by:

$$\delta = \sqrt{\frac{\nu}{\Omega}} \tag{15}$$

There are different sources for what qualifies as a turbulent Ekman boundary layer. Sedney and Gerber [8] used $Re > 10^5$ as the limit for turbulent Ekman layer and Wedemeyer [10] used $Re > 3 * 10^5$ as the limit for a turbulent Ekman layer. It should be mentioned that Wedemeyer only provides experimental data for turbulent Ekman boundary flow at $Re = 6.1 * 10^5$ and laminar Ekman boundary flow at $Re = 1.76 * 10^5$. Sedney and Gerber only made a numerical study on the forming of Ekman boundary layer, but used $Re = 2 * 10^6$ as an example for calculations of turbulent Ekman layers. [10]

The spin-up for a cylindrical tank to steady state flow conditions is given for the laminar case, using impulsive spin-up, by [8]:

$$E_s = \frac{\frac{2c}{a}\sqrt{(Re)}}{\Omega} = \frac{2}{\sqrt{Ek} * \Omega} \tag{16}$$

The derivation of this formula can be found in appendix E.
And in the turbulent case [8]:

$$E_{st} = \frac{28.6 * \frac{c}{a} * Re^{1/5}}{\Omega} \tag{17}$$

However, it is mentioned by Sedney and Gerber [8] that the spin-up times are based on the theoretical work of Wedemeyer [10]. Sedney and Gerber [8] writes: "A rule of thumb is that solid-body rotation is reached at about $4 * t_s$ after an impulsive start of the cylinder", where t_s is spin-up time multiplied by rotational speed. This gives the spin-up time:

$$E_s = \frac{8}{\sqrt{\nu}\sqrt{\Omega}} \tag{18}$$

The Rossby number gives the ratio between inertial forces in the fluid and Coriolis forces. Munk [2] defines the Rossby number as:

$$Ro = \frac{\Delta\Omega}{\Omega_f} \tag{19}$$

Where $\Delta\Omega$ is the differential of initial spinning rate and the final spinning rate and $\Omega_f = \Omega_i + \Delta\Omega$ is the spinning rate after spin-up.[11] The Rossby number for a resting fluid to solid-body rotation would consequently be 1. Weidman [11] suggests that an extension of the Wedemeyer model would give [10]:

$$t_{99} = \frac{\tau_{99}}{2 * \sqrt{Ek} * \Omega} \tag{20}$$

Where τ_{99} is a dimensionless parameter equal to 11.5 for Rossby numbers of 1 for impulsive spin-up of a cylindrical tank. The notation of "99" indicates that every fluid particle has reached 99% of the change in angular momentum.

2.5 Particle Image Velocimetry

To analyze the flow field in both BANNER and LANG a modified PIV was used. The technique used in this report is called "PIV*" (read as "PIV-star"), since it does not contain some of the elements usually seen in PIV-techniques. The technique is implemented by taking pictures of the flow field. The field is seeded with hydrogen bubbles that will follow the flow. The bubbles are then tracked from image to the next images and velocity vectors can be drawn in the path of the bubble.

PIV uses several different algorithms to find the velocity vectors of the flow field, but they all build on the same fundamental algorithm; using a interrogation window and a search window. The Interrogation window is matched against the templates found in the search window. The one window that matches the interrogation window the best is chosen as the new position of the original interrogation window. The difference in position will result in a velocity vector.

The PIV algorithm used in this report is a template matching method using normalized correlation coefficient algorithm. The method can handle large displacements of interrogation windows and is iterative. This means that the method starts with a relatively large interrogation window and

decreases in size every iteration, which gives higher resolution to the flow field. The size of the interrogation window and search window of the normalized cross correlation coefficient algorithm does not require a certain relationship between the iterations, which makes the method flexible.

The normalized cross correlation for a template in two dimensions is given by:

$$\frac{1}{n}\sum_{x,y}\frac{1}{\sigma_f\sigma_t}\left(f(x,y)\right)\left(t(x,y)\right) \tag{21}$$

In image processing $t(x,y)$ is the template, $f(x,y)$ is the subimage, n is the number of pixels in $t(x,y)$ and $f(x,y)$ and σ is the standard deviation.

The velocity vectors are calculated for an area that is chosen on where in the video the least amount of disturbance in the form of parasitic reflection can be found. The velocities are then summarized in the azimuthal direction and averaged over the experimental area. This creates a value that is plotted against time. When the value reaches zero the flow is said to be in steady state. The signal has a certain amount of noise that is filtered using a Savitzky-Golay smoothing algorithm. The algorithm works by fitting a successive sub-sets of adjacent data points with low-degree polynomial the method of linear least squares.

2.6 Scaling

The experiments conducted are scaled to make them easier to perform. The real tank will have a radius of approximately 2.5 meters and the hydrogen has a different viscosity and density than water. It is assumed that the experiments are possible to scale. What should be considered for the experiments in this report is that the Reynolds number is higher in the actual fuel tank. The experiments are meant to verify CFD models that should be able to predict the lower Reynolds number flows and then predict the higher Reynolds number flows and finally predict the cryogenic, micro-gravity high Reynolds number flows of the actual tank.

3 Methods

There were two main methods used to quantify the flow. Several other methods were considered, mostly inspired by Jakob [1], but only two methods gave sufficiently good results. These methods were Image particle tracking and PIV*. The image particle tracking was used for BANNER Half-filled and the PIV was used for LANG and BANNER both Half- and Fully-filled. Each method that was tested is presented in table 1, some of the results were deemed not interesting for the reader, but could be explored in a future project.

Method	**Problems with method**	**Generated Reliable Results**	**Presented in Results**
Using orange Balls to track surface parabola	Balls following flow not remaining at lowest point of surface	No	No
Using Coffee Powder as seeding for PIV	Oil on coffee creating non-water like behavior	No	Yes
Calculating two-dimensional projection of surface parabola	Time consuming since every area needed to measured by hand	No	No
Using Seeds to track surface parabola	-	Yes	Yes
Using Mica powder to visualize flow	Difficult to quantify flow, not usable on laminar flow	No	No
Using seeds as seeding for PIV	Seeds clump together in the middle, not showing the flow at the edges.	No	No
Using hydrogen bubbles as seeding for PIV	Different types of bubbles, creating their own flow	Yes	Yes

Table 1: The different methods tested and the reliability

3.1 Image Particle Tracking

To examine the spin-up time for a tank reaching steady state with a open surface, the shape of the surface can be tracked to determine steady-state flow. The theoretical values for the shape of the parabola can be compared to experimental measurement to determine when the flow reaches solid-body rotation.

The method of Image Particle Tracking uses a video of spin-up of the tank and analyses each picture to determine the shape of the parabola. The tank is filmed from the side with the camera aligned with the open surface of the water for the fluid at rest. The fluid is then spun-up and the images are processed. On the surface of the water, seeds of sunflower are distributed. The sunflower seeds are roasted which gives them a dark black color. This makes them ease to identify using image analysis. As can be seen in figure 5 the seeds are the darkest pixels in a certain area. The picture is a matrix of values between 0 and 255, where 0 represents black and 255 represents white. The seeds on the bottom of the tank will be swept away by the Ekman pumping as the spinning starts and the seeds at the surface will be gather at the middle due to Ekman pumping.

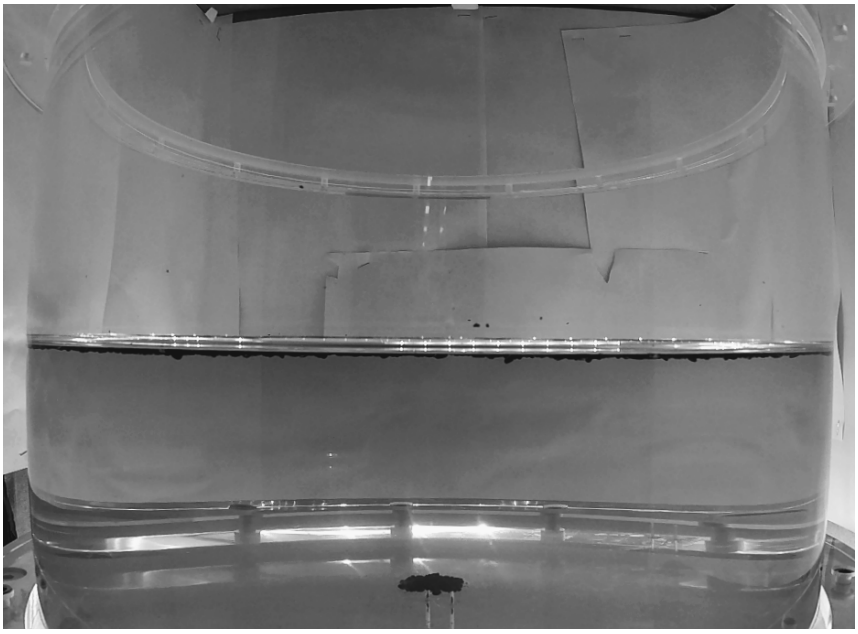

Figure 5: BANNER Half-filled, fluid at rest

The image is subjected to a threshold so only values of 0 and 255 are present in the matrix, see figure 6. An arbitrary coordinate system is drawn out and a search algorithm is implemented. The algorithm finds the lowest point where a pixel with zero value is present and stores this value for every image. This algorithm is performed on every picture in a ten minute long video which makes it possible to plot the transient development of the position of the lowest point of the parabola.

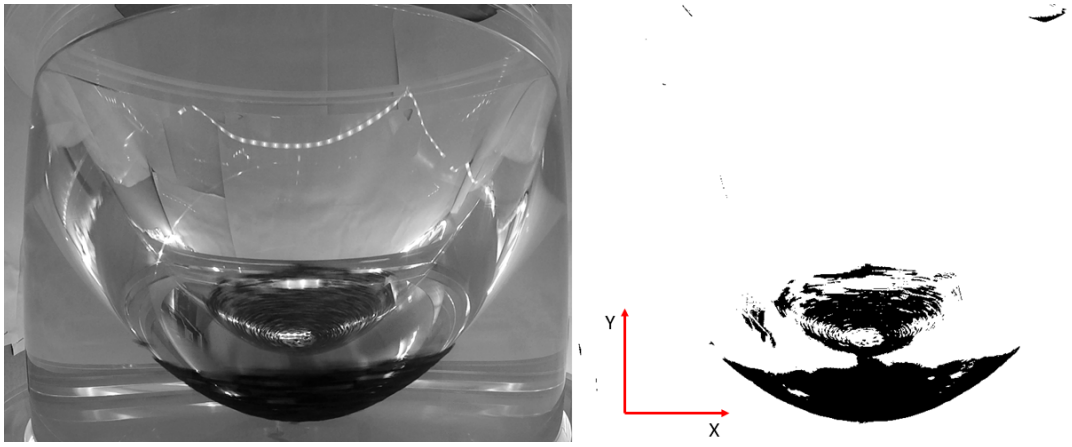

Figure 6: **Left**:Picture of the parabola forming for a spinning fluid. **Right**: Picture subjected to threshold

In figure 7 a plot of the position of the lowest point of parabola is shown. Note that the theoretical value for the lowest point of the parabola in steady state is 49 mm, according to equation 7. The plot is smoothed using "loess" smoothing. The smoothing window is set to be relatively large to make sure that the derivative of the smoothed function reaches zero as the true position of the vertex oscillates around the steady state value. The method is not perfect which means there will always be disturbances in the flow. These disturbances are omitted in the smoothed function. The flow reaches steady state as the derivative of the smoothed function gets close to zero.

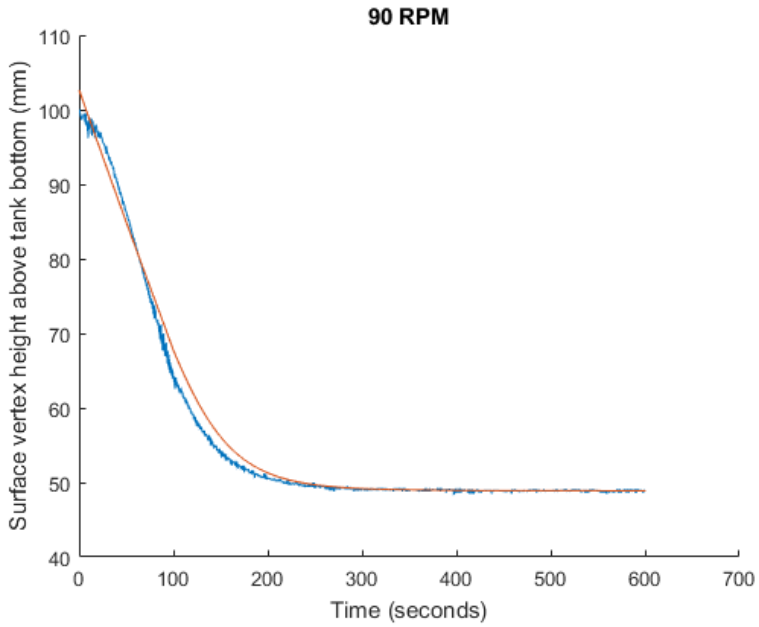

Figure 7: The development of the parabola. The blue line represents the unmodified position of the surface vertex and the red line is a loess smoothing

3.2 PIV*

All the experiments conducted in this report have been subjected to analysis using PIV*. The method is based on the PIV algorithm for analyzing flow, but the conventional version uses a laser. The particles are instead illuminated using LED-lights. This gives a relatively large area of illumination, but the particles are contrasted against a black background which will give relatively high quality pictures.

The first camera used was a GoPro Hero 4, but the resolution turned out too be to low for the small particles in the flow. The camera used for the experiments was the mobile phone camera on a Huawei P9 which could film at 30 frames per second. This gives an indication of the order of magnitude of the shutter speed of the camera, which should be around $1/30s$.

Several different tracing particles were tested with different results. Coffee powder turned out to give good contrast and good measurements. However, the coffee turned out to affect the behavior of the water and could not be used on a tank that did not have a open surface. The sunflower seeds where used and gave a better result, but could still to be used in a closed tank. The flow was seeded using hydrogen bubbles created with electrolysis which generated more accurate results.

The flow was filmed from above or from below depending on which tank was used and on which seeding method was used. The video was converted into images using the software FFMPEG and each set of two images was analyzed to calculate the velocity vectors in the field. The images was subjected to a threshold to generate a picture with only black and white colors. For some of the images an algorithm was used to subtract some of the background lightning to generate a picture with higher contrast

Figure 8: Unmodified picture of bubbles, filmed from below the tank

Figure 9: The two modified images for the PIV, taken with 0.2 seconds interval

The PIV algorithm was executed for three iterations with interrogation window getting smaller for each iteration. The window started at 150x150 pixels, then 75x75 pixels and lastly 25x25 pixels. The results can be seen in figure 10. The results are given in pixels which means they need to be converted to m/s.

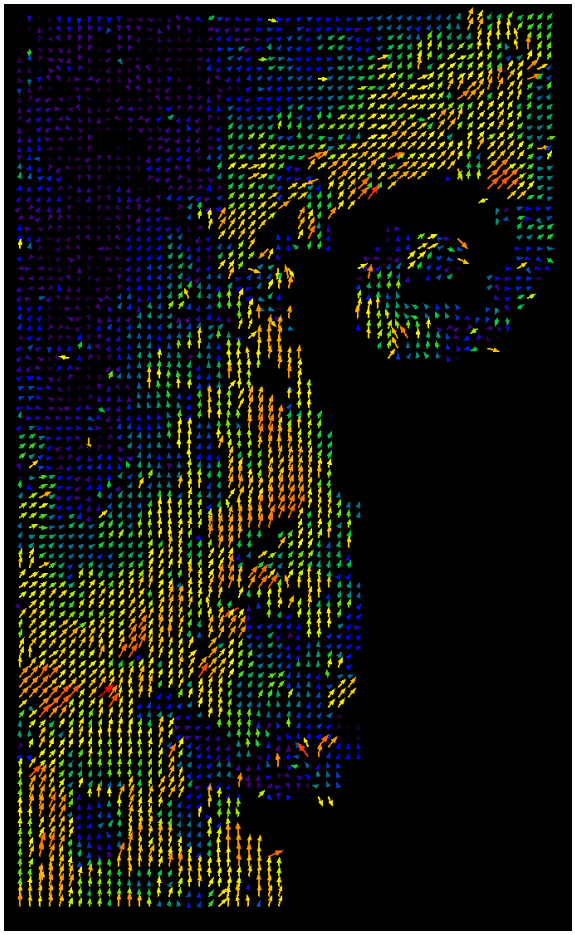

Figure 10: Velocity vectors for the PIV*

The PIV gives the velocity in x- and y-direction and plots the velocity vectors using Pythagoras theorem. In some of the results cylindrical coordinates are used and only the velocity in θ- direction is accounted for, see figure 1.

To visualize how the flow field develops over time, the velocities in a certain coordinate direction are summarized and plotted over time. This gives data over a larger surface than only plotting the velocity in one point and makes the impact of noise (incorrect measurements) smaller in the results.

3.3 Bubbles

The electronics behind electrolysis was designed and tested by Jakob [1]. The water is mixed with sodium bicarbonate. A DC current is driven through the wires which induces a chemical reaction in the system. At the cathode hydrogen gas is created and at the anode, oxygen gas is created. The setup can be seen in figure 11 and 12. The bubbles of interest are the hydrogen bubbles since they are created at a higher rate than the oxygen bubbles.

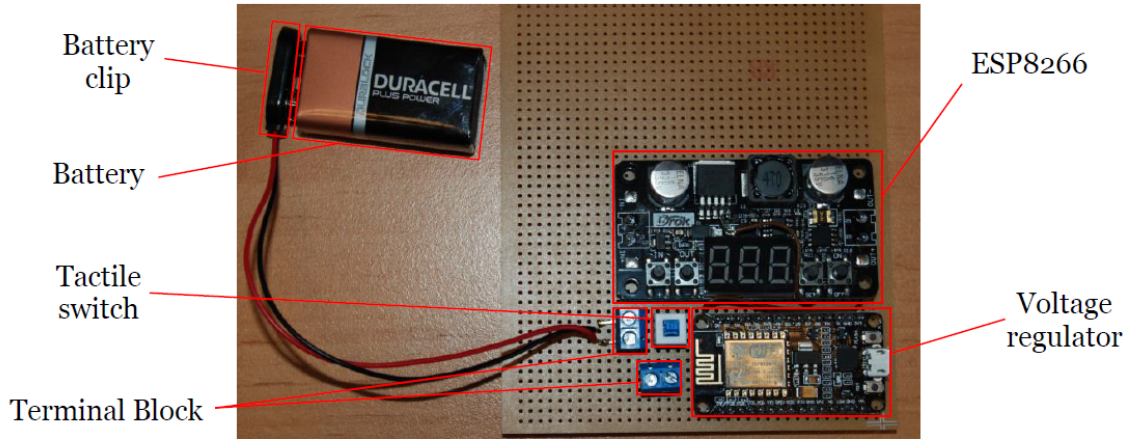

Figure 11: The way the wires are connected in the electrolysis device (top), Picture by Jakob [1]

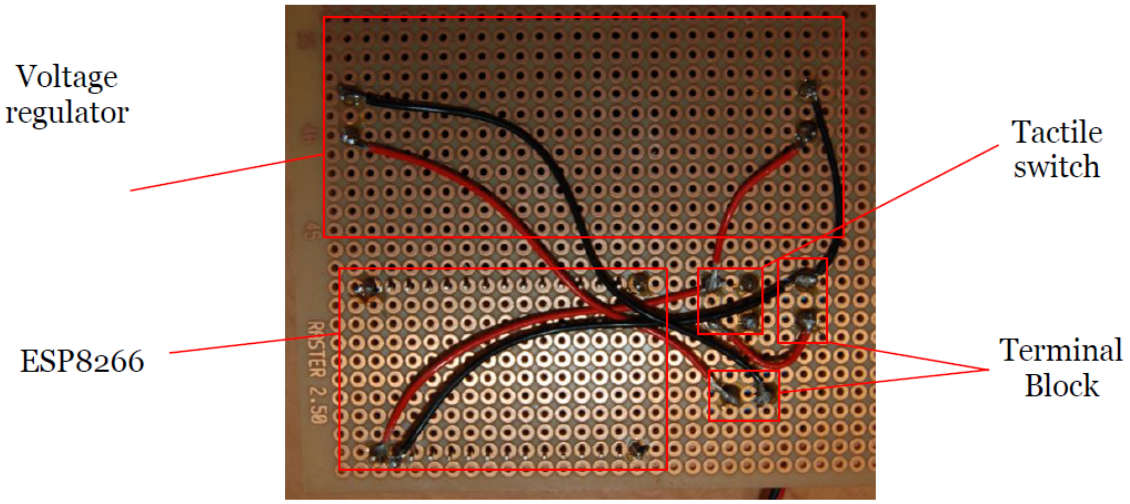

Figure 12: The way the wires are connected in the electrolysis device (bottom), Picture by Jakob [1]

The trajectory and shape of the bubbles are complex to calculate and predict, see appendix B. The bubbles were created in two distinct characteristic types. One type were bubbles that attached to the wire and grew until they gain enough buoyant force to detach from the wire. These bubbles were bigger and rose fast to the surface. The velocities of the bubbles were in the same order of magnitude as theory would predict. The other type of bubbles were smaller bubbles detaching from the wire almost instantly as they are created. These rise slowly to the middle of the tank and are diffused after 30 seconds. These bubbles are more useful for the experiments since they can be seen for a longer period of time. It was also concluded that the distance between the wires are not important inside the tank and that the flow created by the bubbles is negligible, see appendix B.

The bubbles were filmed with a camera mounted below BANNER. The camera rotated with the tank, since it was mounted of the frame. The spin-up time for reaching steady state was determined using two different methods. The first one visually measured the time until most bubbles started rising straight up from the wire, see figure 13. Note that the picture of the steady state almost shows a bubble flow to the right, this is only due to the offset of the camera showing the lamina of bubbles from the side. To see more on how the visual measurement of steady state was made, see video referenced in section A.3.

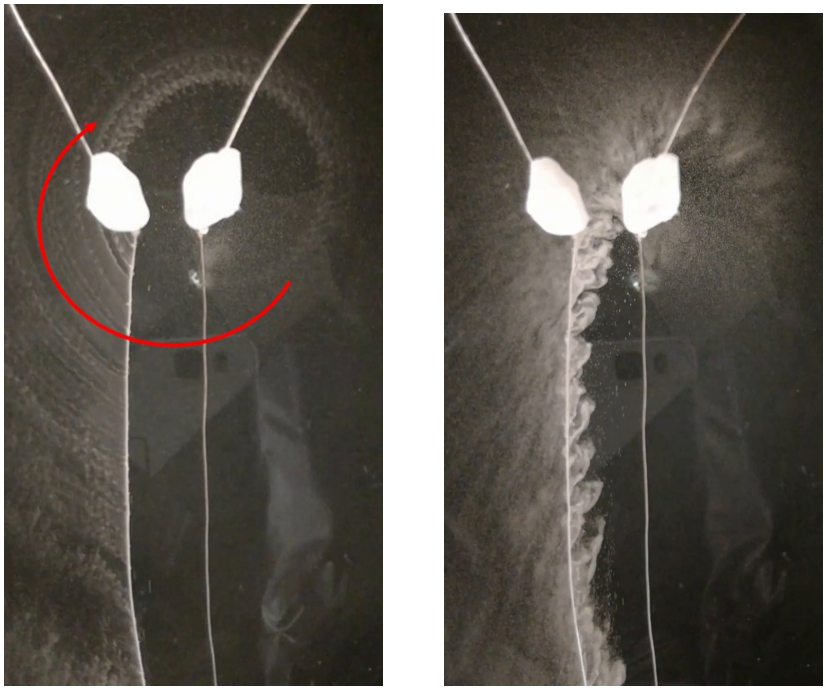

(a) Non-steady (b) Steady

Figure 13: Bubble-formation for unsteady and steady flow, with the same view as seen in figure 8.

3.4 Normalizing the results

To make the results more tangible, some of the results from the velocity measurements were normalized. The normalizing divisor is obtained by integrating the solid-body rotation velocity profile for a given area. This means that the velocities in an area are summarized and normalized with the value of the velocities in the same area for a cylinder with a radially linear velocity profile. The value of the integrated solid-body rotation velocities is called the mean velocity for that specific area.

4 Set-up

Three sets of experiments were conducted. First experiments were PIV* experiments that were conducted on LANG, half-filled with water, using tracing particles to seed the flow. The second set of experiments were image analysis of the parabola in BANNER, half-filled. The third set of experiments were PIV* experiments on BANNER using a filled tank.

4.1 LANG Half-filled

LANG is made out of acrylic plastic. The tank is mounted on a frame that allows it to be accelerated laterally, which will not be used in this project. The tank is driven by an engine mounted on top of the tank which is secured by a framed made out of aluminum. The inner diameter of the tank is 192 mm and the inner height is 257 mm. The setup can be seen in figure 14.

Figure 14: Setup for experiments, picture by Jakob [1]

LANG was modified to allow for a camera to film the fluid from above and to allow wires to be inserted into the tank. The top was cut off and replaced with an aluminum lid which could be mounted with an electrolysis device designed by Jakob [1] and a counter weight, see figure 15.

Figure 15: LANG with modified lid

The tank was filled to the half-height with water and the surface was covered with coffee powder to seed the flow. The flow was analyzed using PIV*.

4.2 BANNER Half-filled

BANNER is made out of machined acrylic plastic. The measurements for the tank can be found in figure 16.

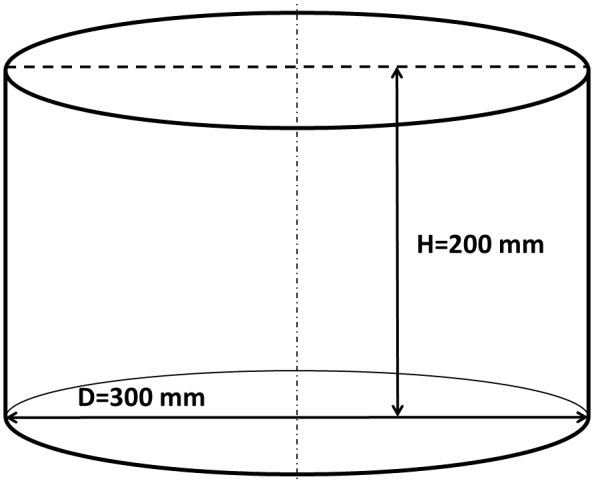

Figure 16: Measurements of BANNER

The tank is mounted on a base plate which is mounted to a experimental table using four dummy sliders. The tank is mounted on a bearing which has an axis connected to a cogwheel. The cogwheel is connected to the motor using a chain, see figure 17 and 18. There was a structure suggested for the tank that would mount a bearing on top of the tank. This structure was not used, see figure 18. Note that the GoPro was not used, instead it was replaced with a mobile phone camera. The GoPro was mounted on a structure to film the cylinder from the side and track the surface parabola.

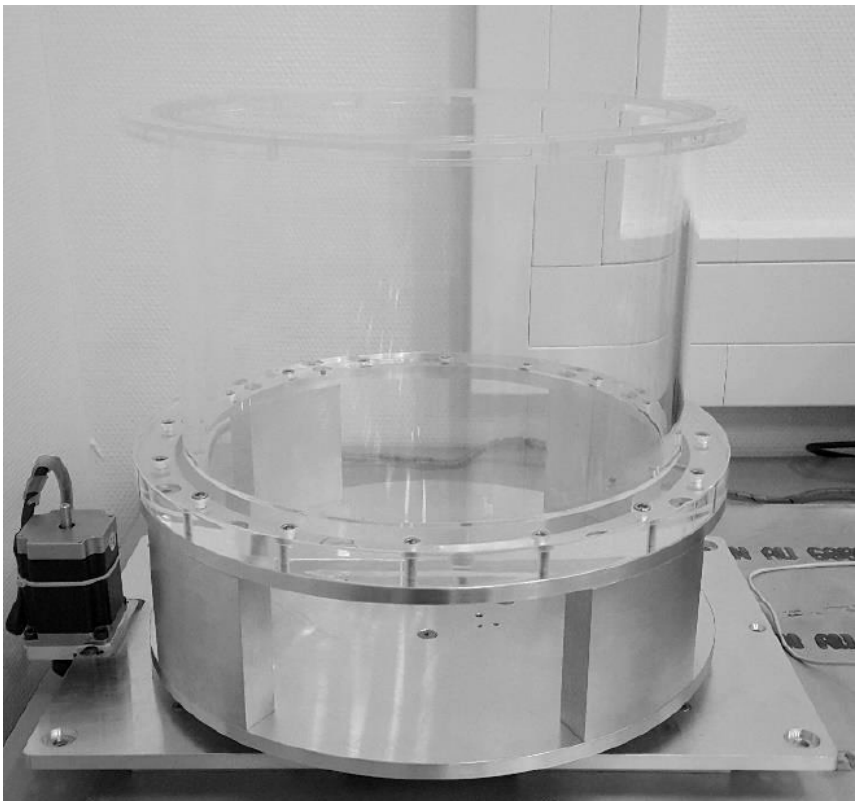

Figure 17: BANNER

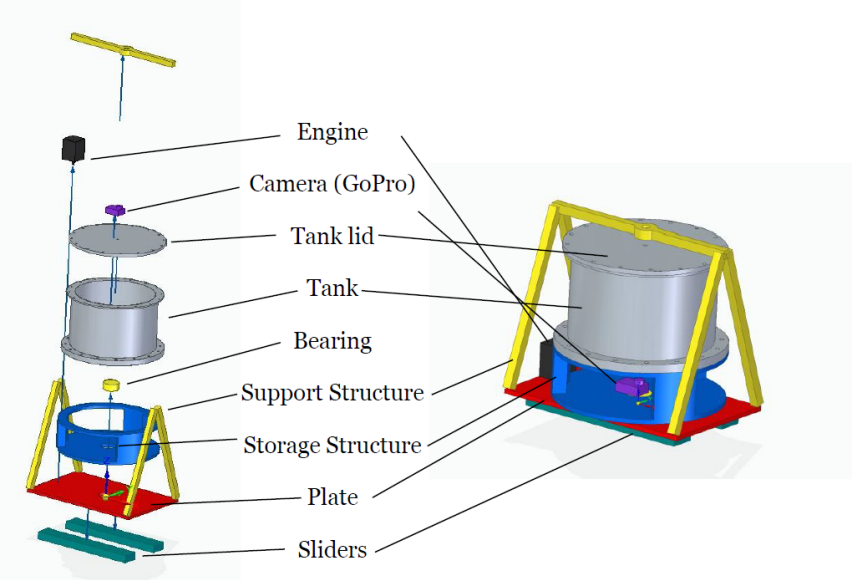

Figure 18: Schematic setup of BANNER. Note that several parts are not in the final version of the tank.

The setup for BANNER Half-filled can be found in figure 18. The camera is mounted a cardboard box, filming the tank from the side. The camera is aligned with the surface of the water. The cardboard box on which the camera is mounted on is equipped with LED-lights on the the bottom edge, which illuminates the room created by the box. It can be seen how Jakob [1] had some trouble with reflecting light from light sources in the lab. The box is supposed to eliminate all light sources beside the LED-light. The box is not equipped with a lid, the argument for this being that the surface wave should be dampened out by the surface tension of the water, see equation 10.

The tank is spun up using a NEWA23 stepper motor with 1.89 Ncm in holding torque. The motor has a controlling software to control spin-up acceleration, spin-down deceleration and spinning rate.

BANNER is filled with water to the half height of the tank, which is 100 mm. The camera is aligned with the water surface. The surface is then covered in sunflower seeds.

The experiments were repeated several times to ensure that the results were coherent. Several different rotational speeds were examined to determine a correlation between spin-up time and rotational speed. The tank was spun for 10 minutes to ensure steady state.

Since the experiments were going to be compared to CFD, the acceleration period is optimized to be as short as possible. This is to ensure that CFD has to simulate a shorter time of acceleration and lower the cost of each computation, since only the spin-up time is of importance for this project. The moment of inertia is approximated with the moment of inertia for a solid cylinder. The mass of the cylinder is approximately 20 kg, depending on the amount of water in the tank. The radius is 150 mm and the torque of the engine is 1.5 Nm for a rotational speed of 105 RPM. This torque was used as an reference value. [15]

$$a_\theta = \frac{M_\theta}{I_\theta} = \frac{M_\theta}{r^2 * m} = 3.33 rad/s^2 = 190 \deg/s^2 \tag{22}$$

To ensure that the engine will be able to handle the torque, and acceleration of $100 \deg/s^2$ was chosen as acceleration and $60 \deg/s^2$, since there was less importance on fast de-spin.

4.3 BANNER Fully-filled

The schematic setup for BANNER can be found in figure 18. The tank is filled with water and mounted with a lid. The lid is mounted with screw and bolts and fitted with a sealing ring to make

sure the water does not leak out of the tank. The tank is supplied with a storage area below the acrylic tank, which holds the electrolysis machine and the camera, see figure 19. Both instruments are mounted using duck tape.

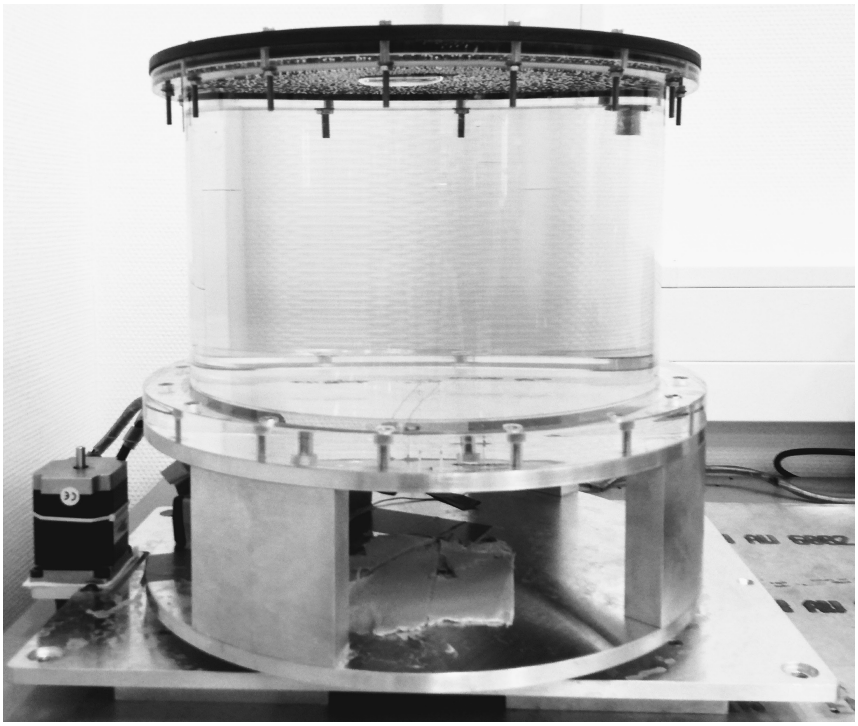

Figure 19: BANNER with the lid

The electrolysis machine has two wires, one anode and one cathode, which are inserted into the tank. The tank has drilled holes in the bottom to fit the wires through. The wires are inserted in one hole in the middle and secured on the outside of the tank close to the edge of the tank. The holes are sealed to ensure that the water does not leak out.

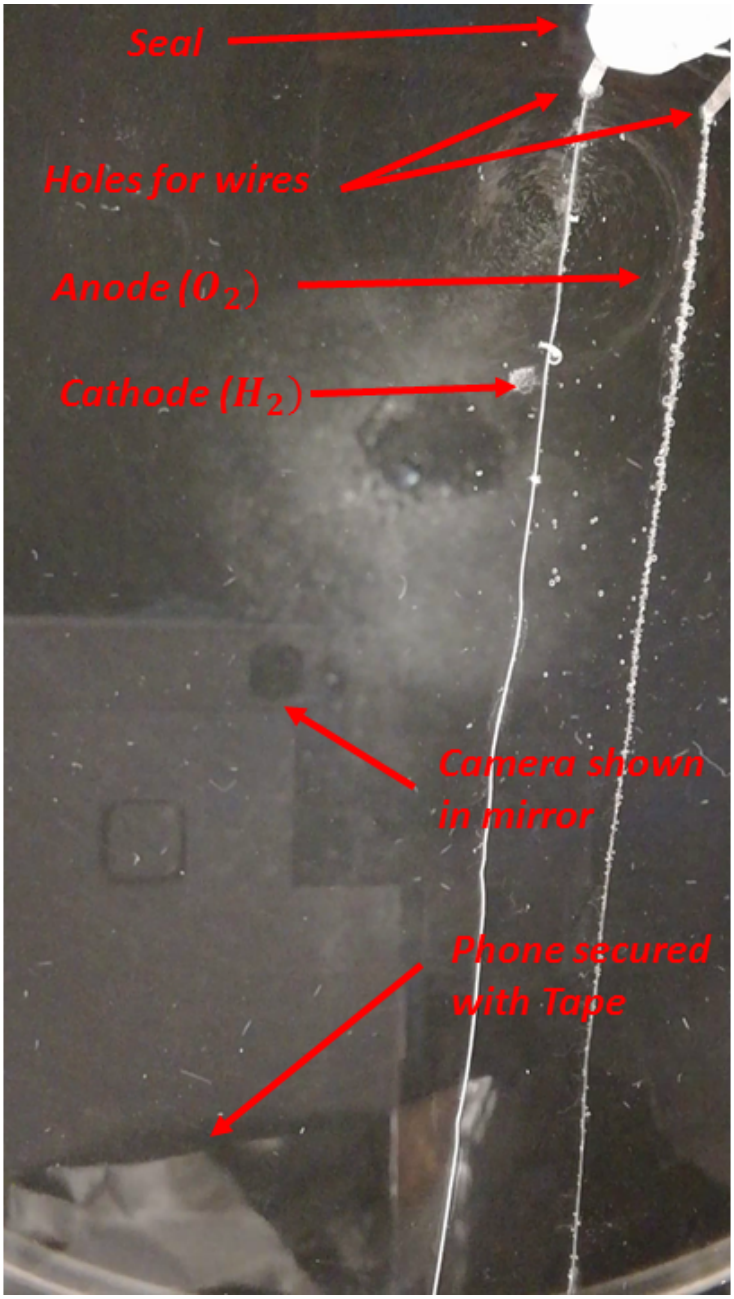

Figure 20: BANNER seen from the sloth under the tank. Wires and configuration shown

The experiments were conducted on several rotational speeds. The acceleration was the same as for the experiments on BANNER with open surface. The tank was spun for 10 minutes to ensure that the fluid reaches steady state.

5 Results and Discussion

5.1 LANG Half-filled

LANG was analyzed using the particle image velocimetry. The tank was spun-up to 80 RPM using an acceleration of 200 deg $/s^2$.

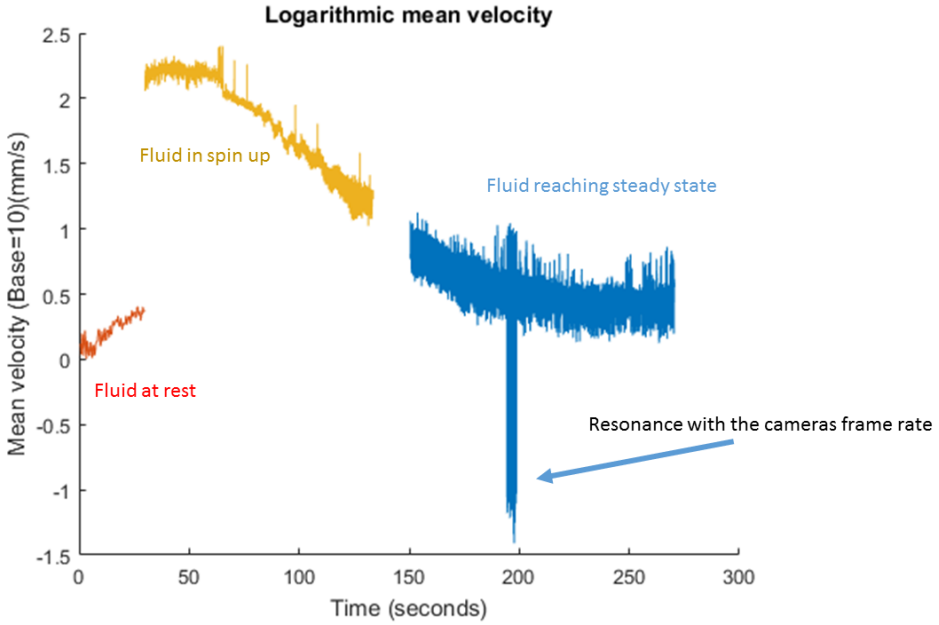

Figure 21: Logarithmic development of the mean velocity in LANG

The velocity as a function of time was plotted and when the signal reached a steady mean value, not regarding the noise, the fluid was said to be in steady state. The value is around 220-240 second which can be compared to Jakob [1] visual data that had a spin-up time of around 240 seconds. It should be noted that her tests were only based on personal estimation of visual evidence, not analyzed using any image-analysis tool.

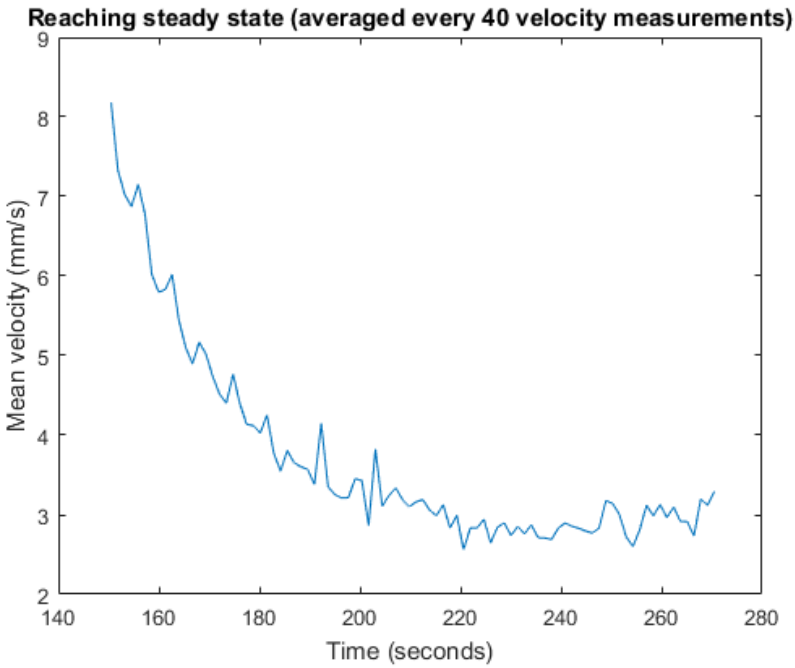

Figure 22: Close up of the mean velocity as the fluid reaches steady-state, smoothed function

There is a residual velocity even as the velocity as function of time reaches a steady mean value. In the video A.1 this can be seen as a the particles oscillating back and forth. This is also seen in the Fourier transform of the signal, where the rotational speed is seen as dominant frequencies. This is believed to be due to a malfunction in the engine of bearing that causes the tank to decrease in speed once every rotation.

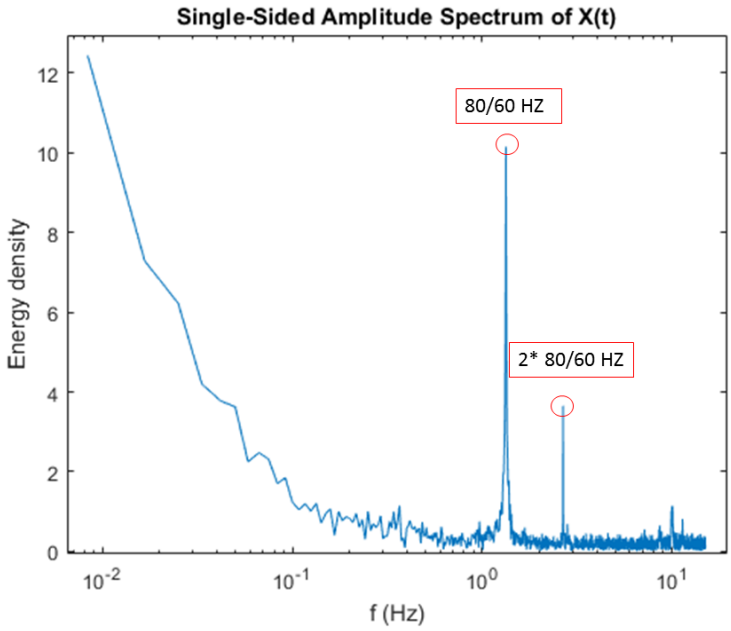

Figure 23: The single-sided Fourier spectrum of the mean velocity as a function of time

5.2 BANNER Half-filled

The test-plan was designed to measure the spin-up time for several rotational speeds and determine a relation between rotational speed and spin-up time. The acceleration was chosen to 100 deg $/s^2$ for each test case. The tests were divided into two categories, resting fluid and non-resting fluid. The category of resting fluid were tests conducted on the fluid when the mean velocity of the surface flow was below 5 mm/s before the rotation was initiated. The mean velocity was measured using PIV*, seeded with sunflower seeds. For the non-resting fluid, the mean velocity of the surface was above 15 mm/s.

Initial state	**Rest**	**Non-Resting**	**Rest**	**Non-Resting**	**Rest**	**Non-Resting**
RPM	**30**	**30**	**60**	**60**	**90**	**90**
Test 1, mm/s	0.9	19.7	0.3	14.7	1.9	18.3
Test 2, mm/s	3.9	20.8	1.8	19.0	0.5	19.2
Test 3, mm/s	2.2	20.1	0.1	18.5	0.1	18.6
Test 4, mm/s	0.7	19.4	6.1	18.5	0.3	19.4
Test 5, mm/s	0.8	19.4	7.2	18.2	0.8	18.7

Table 2: Different initial mean velocities at the surface of fluid

The results of the initial test are plotted in figure 24 and figure 25. The plots show the mean values for five tests on resting and five tests on non-resting fluid for the rotational speeds of 30, 60 and 90 RPM. The spin-up time is calculated using the derivation of the coordinate of the lowest point of the parabola as a function of time and can be found in appendix C.

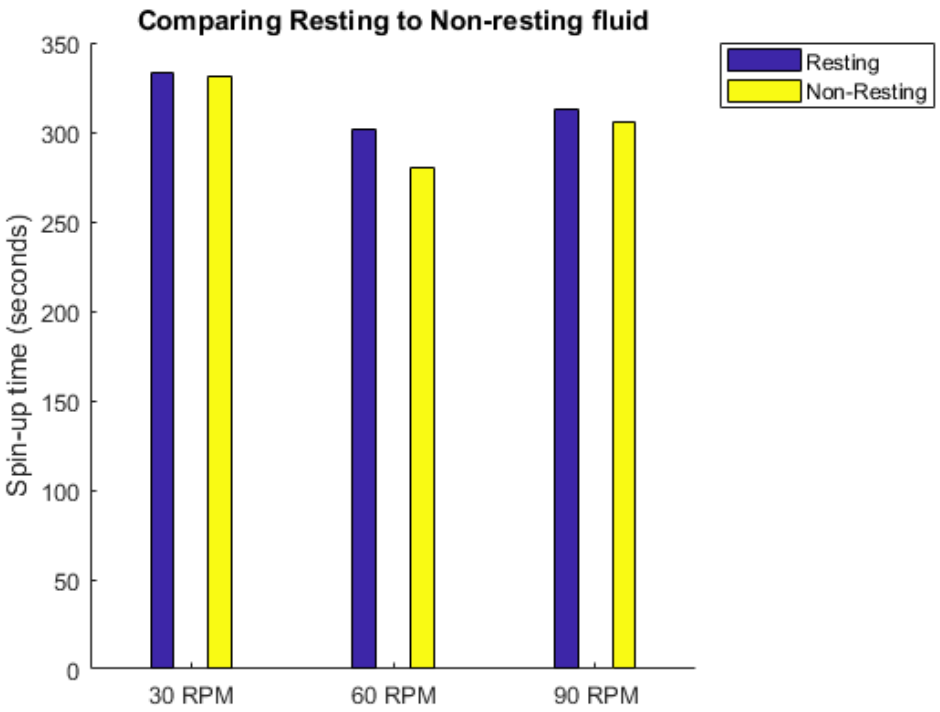

Figure 24: Mean value for the spin-up time for different rotational speeds with resting and non-resting fluid

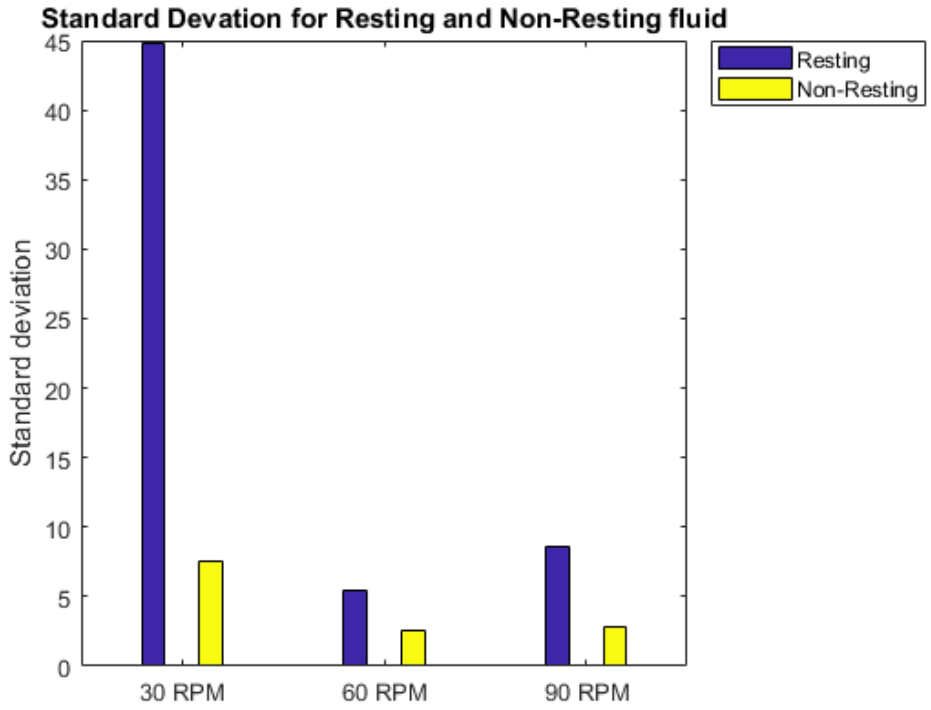

Figure 25: Standard deviation for the spin-up time for different rotational speeds with resting and non-resting fluid

From these measurements it was concluded that all tests should be made on a initially resting fluid. The spin-down was analyzed using the same technique as the spin-up. It was found that the

spin-down time was mostly unaffected by the rotational speed. The spin-down acceleration was the same for all test cases. The typical spin-down can be found in figure 26. When the coordinate of the y-position reached zero the fluid was said to have reached a zero pressure gradient steady state. This indicates the centripetal force is too weak to affect the pressure gradient. The time until the y-coordinate for the lowest point of the parabola reaches zero can be found in table 3. The surface still had some velocity that decreases with time. The plot for the surface mean velocity can be found in figure 27. The time until the fluid is considered to be at rest is chosen to 360 seconds, which is double the time found in figure 27. This is to make sure there are only a small amount of residual kinetic energy present in the fluid.

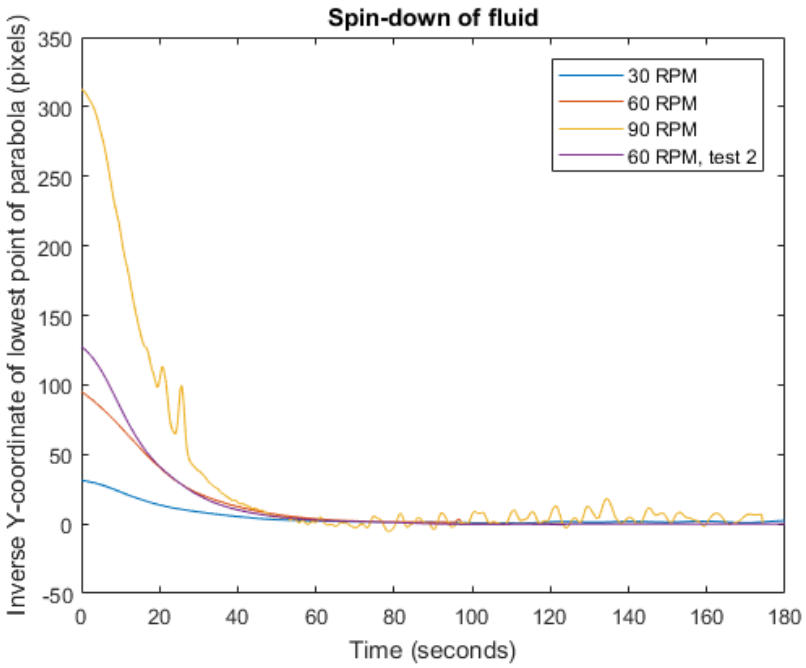

Figure 26: The development of the lowest point of the parabola over time during spin-down

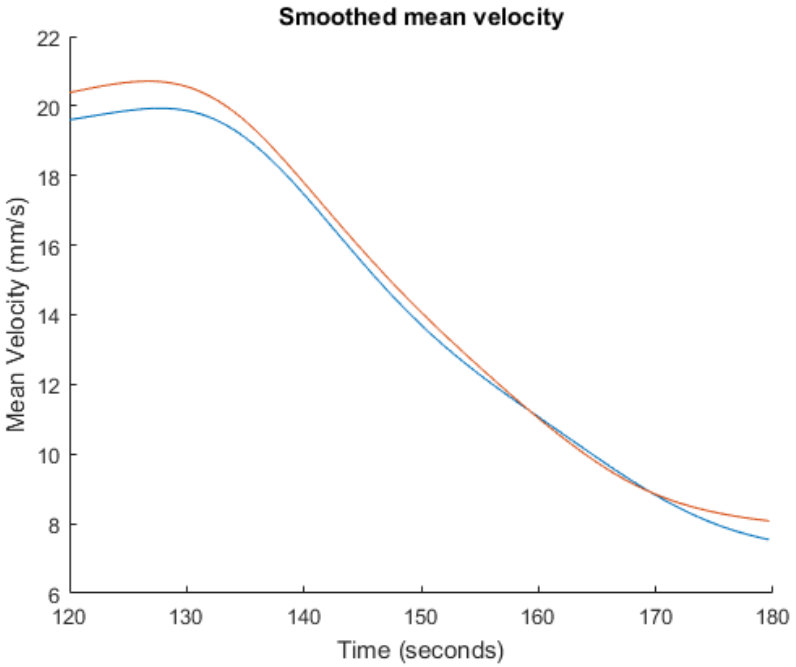

Figure 27: Mean velocity in on the surface as a function of time. Two measurements are displayed to show repetability.

	30	**60**	**90**
Test 1	63.33333	60.66667	62
Test 2	55.66667	62.33333	64.33333
Test 3	61.66667	63	60.33333
Test 4	67.33333	61	62.66667
Test 5	63.33333	61	61.66667
Test 6	-	61.66667	-
Test 7	-	60.33333	-
Test 8	-	57.66667	-
AVG	**62.26667**	**60.95833**	**62.2**
STD	**4.23871**	**1.59799**	**1.464392**

Table 3: Spin-down times for zero Pressure Gradient steady-state

The test case can be found in table 4. The number of tests was chosen somewhat arbitrarily. There was an idea to perform a certain number of tests for each case, but not all data turned out to be of good quality. In some cases, the sunflower seeds would detach from the surface of the water and float in the middle of the fluid, being neutrally buoyant. This would ruin the test and the data could not be used. 60 RPM was studied in a wider extent since 60 was one of the rotational speeds chosen to be compared to CFD.

RPM	**Number of tests**	**Average**	**Standard deviation σ**
30	5	333	44.8
45	4	267.5	12.9
60	13	292.9	8.7
75	2	276.5	15
90	11	308.7	22.4
105	6	274.3	42.3
120	5	264.2	6.9

Table 4: Table showing the test case and the results

A bar plot can be found in figure 28 of the same results found in table 4.

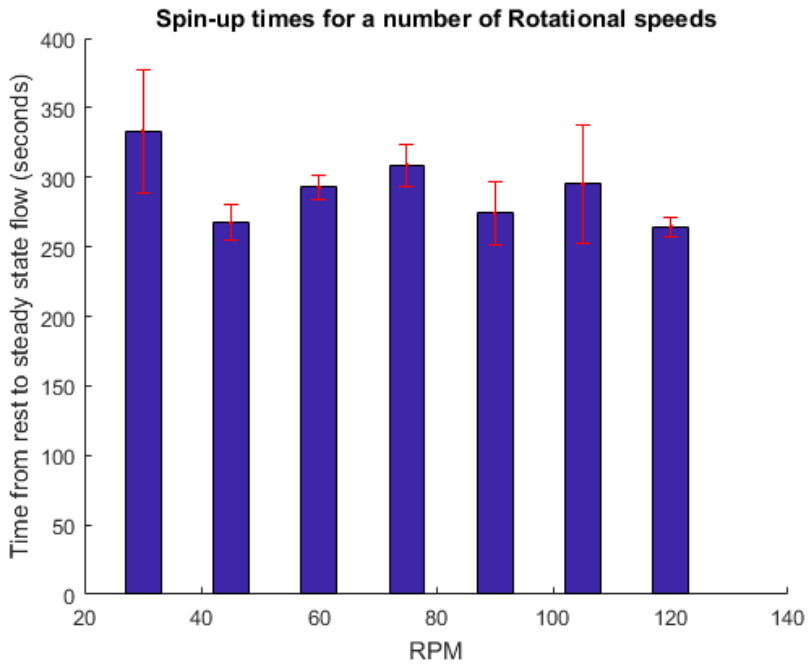

Figure 28: Spin-up times for different rotational speeds, the red lines have the lenght of two σ

5.3 PIV* on LANG Half-filled, using Coffee

The surface of the tank was covered with a powder of coffee and the velocity field was quantified using PIV*. The technique was only used for two tests since the experiments showed that the coffee was affecting the results of the experiments. The coffee powder is covered in an oily substance that affects the surface tension of the water. This can be seen when pouring on the coffee on the water, how the coffee powder spreads out over the surface without being affected by external forces. The time until steady state found in figure 29 is 283 seconds. The time is calculated by finding the time when the Savitzky-Golay filtered function reaches zero velocity for the first time. This result is reasonable compared to the method of tracking the lowest point of the surface parabola.

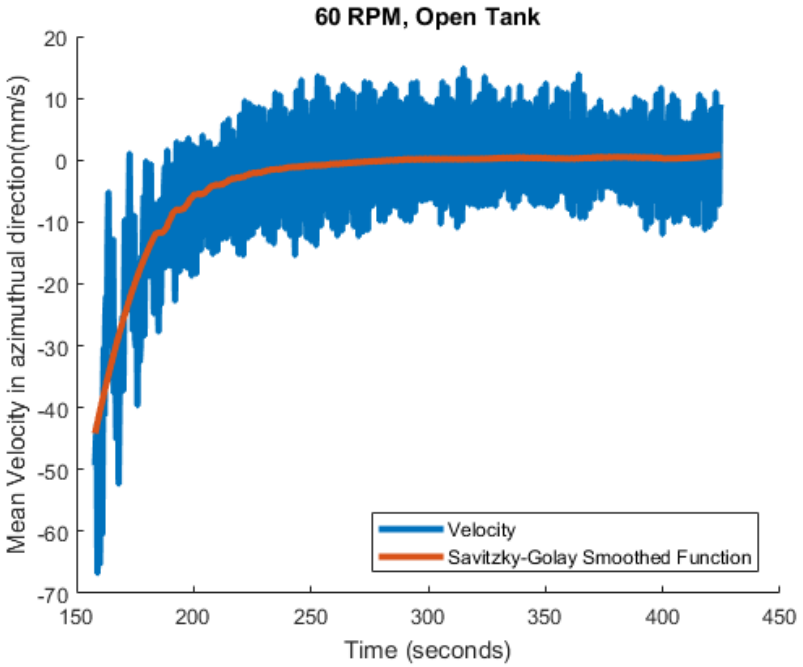

Figure 29: Azimuthal velocity as a function of time, using PIV* with Coffee as seeding.

The second test showed an nonphysical behavior of the velocity field. The plot is different from the plot seen in figure 29 in the way that it shows the absolute value of all the velocity vectors averaged over the experimental area as a function of time. The function initially behaves as expected but is then brought to a sudden halt. After a while the noise returns and the function continues as expected. This behavior is also verified on the video, where the entire field is seen to stop at t=200 seconds and the movement slowly coming back at t=300 seconds. This is believed to be due to the coffee affecting the surface tension of the fluid and thereby dampening some of the Kelvin-Helmholtz instabilities created by the shear-layer between the water and the air, see equation 10.

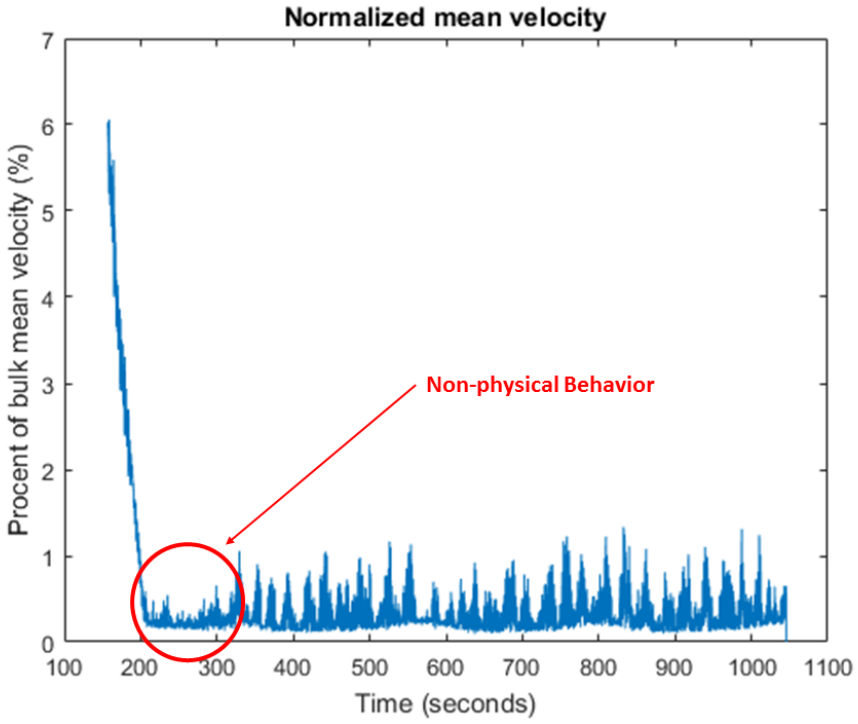

Figure 30: Absolute value of the velocity as a function of time, using PIV* with Coffee as seeding.

5.4 PIV* on BANNER Half-filled, using Bubbles

The results seen in table 4 is verified using PIV* on hydrogen bubbles. There were two ways to quantify the flow using the hydrogen bubbles. The first was to visually inspect the video of the bubbles and determine when the majority of the bubbles were rising straight up from the wire and use this time as the time until the flow reaches steady state. The second method was using the PIV*-method to determine a mean velocity over a certain area and plot this velocity as a function of time. Since the camera is rotating with the frame of the cylinder, when the velocity in azimuthal direction reaches zero, the flow is said to be in steady state.

RPM	Spin-up time (visual)	Spin-up time (PIV*)
30	450	420
60	-	420
90	-	-

Table 5: Spin-up times for different rotational speeds for BANNER Half-filled. The "-" shows when a spin-up time could not be determined.

5.5 BANNER Fully-filled

The movies created from the test of BANNER Fully-filled were analyzed the same way as for the tests on BANNER Half-filled. The movies were analyzed both visually and using PIV*.

RPM	Spin-up time (visual)	Spin-up time (PIV*)
30	420	442
60, test 1	320	340
60, test 2	326	338
90	270	290
200, test 1	190	198
200, test 2	190	180
360	140	130

Table 6: Spin-up times for BANNER Fully-filled at different rotational speeds.

The results from table 6 are plotted in figure 31. The results from the measurements are plotted together with theory from Sedney and Gerber [8] and Weidmann [11]. Note that the theoretical value for spin-up time for Sedney and Gerber is just a factor 4 times larger than the value derived by Wedemeyer [10]. The results of the experiments fit well with the theory for laminar Ekman boundary layer flow.

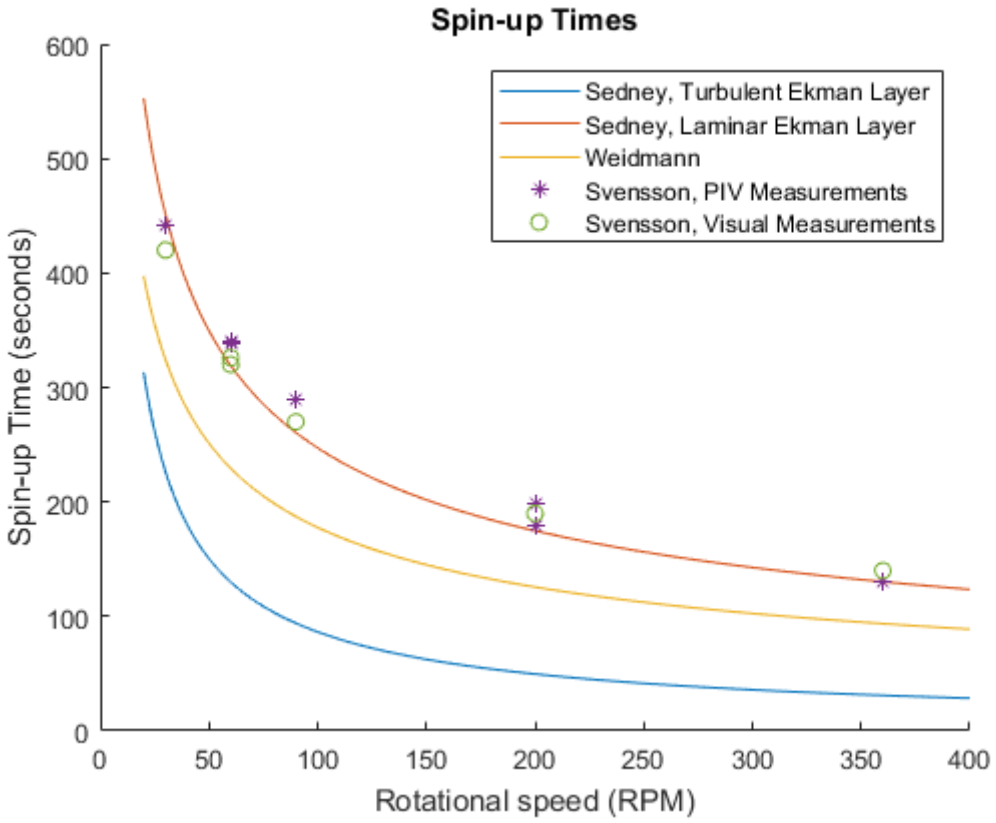

Figure 31: Spin-up times for given geometry.

6 Conclusion

6.1 BANNER Half-filled

The spin-up time measured for the pressure steady state are considered fairly accurate relying on the theory of spinning tanks. The method is not verified using any other method, since no theoretical spin-up times are calculated and currently no CFD experiments are considered reliable. The measurements on BANNER Half-filled using PIV* can not be used as verification since they use the velocity as a measurement of steady state. The velocity in the tank is seen to oscillate due to the shear layer created by the water and the air, which gives a slow spin-up time, seen in the PIV*-measurements using bubbles as seeding. The first test using coffee seemed promising, but it

was discovered in the second test that the coffee affects the experiments, which makes the method unreliable.

The tests of the spin-up time for the steady state pressure can be seen as verification data for future work. The spin-up times vary from test to test and created a relatively high standard deviation. There is no direct link between rotational speed and spin-up time. All rotational speeds spin-up at similar rates. This is believed to be due to how the water surface interacts with the air and creates disturbances in the flow. The only test for LANG indicates a spin-up time that is faster, but since there is only one test, the data is not statistically significant.

6.2 BANNER Fully-filled

The experiments show a close resemblance to the theory on laminar Ekman boundary flow suggested by Sedney and Gerber [8], see figure 31. This indicates both that the theory of Sedney and Gerber [8] and the experiments are accurate to determine the spin-up time for a rotating cylindrical tank filled with water. According to Sedney and Gerber the experiments should give turbulent Ekman boundary layer flow, which they clearly do not. This is believed to be due to the slow acceleration maintaining laminar Ekman boundary layer flow through-out the spin-up period, never creating turbulence. Wedemeyer [10] presented results on experimental data verifying theory for turbulent Ekman layer boundary layer flow, where the tank was accelerated almost instantly. This indicates that the amount of turbulence in the tank is determined by the acceleration of the flow, not the final rotational speed.

7 Further Work

The main focus on further work would be to increase the acceleration of the rotation of the tank, so to initialize turbulence in the Ekman Layer. If the it could be shown that Sedney's and Gerber's [8] theory for turbulent flows is correct, this could give data on significantly faster spin-up times. Test could also be conducted to examine when the flow is transitioning to turbulence.

8 References

References

[1] Henrike Jakob, *Final Report Henrike Jakob*. European Space Research and Technology Centre, Noordwijk, 1st Edition, 2017.

[2] Johannes Munk, *Numerishe Untersuchungen von rotierenden Flüssigketien mit dem DLR THETA code*. Munich Technical University, Munich, 1st Edition, 2016.

[3] ESA, *ESA webpage*. http://m.esa.int/ESA, retrieved 2018-02-12

[4] ESA web page, *Ariane 6 rocket. https : //web.archive.org/web/*20170225174215/*http : //m.esa.int/Our*$_A$*ctivities/Launchers/Launch*$_v$*ehicles/Ariane*$_6$, retrieved 2018-02-12

[5] Arianspace, *Ariane 6*. issue 0 *https : //web.archive.org/web/*20170214115631/*http : //www.arianespace.com/wp − content/uploads/*2017/02/*Ariane*6$_U$*sers − Manual*$_F$*ebruary*2017*.pdf*, retrieved 2018-02-12

[6] Raouf A. Ibrahim, *Liquid Sloshing Dynamics: Theory and Applications*. Cambridge University Press, Cambridge, 1st Edition, 2005.

[7] Sebastian Schmitt, *Experimental and Numerical Investigation of Two-Phase Flow with Non-Isothermal Boundary Conditions under Microgravity Conditions*. Bremen University, Bremen, 1st Edition, 2016.

[8] Raymond Sedney, Nathan Gerber *OSCILLATIONS OF A LIQUID IN A ROTATING CYLINDER: PART II. SPIN-UP*. Us Army Armament research and Development Command, US, 1983.

[9] H.P. Greenspan *THE THEORY OF ROTATING FLUIDS*. Cambridge 1968.

[10] E. H. Wedemeyer, *The unsteady flow within a spinning cylinder*. U.S.A Ballistic Research Laboratories, Aberdeen, 1st Edition, 1964.

[11] Patrick D. Weidman *On the spin-up and spin-down of a rotating fluid. Part 1. Extending the Wedemeyer model*. Department of Aerospace Engineering, University of Souther California, Lose Angeles 1975.

[12] Imperial College London, *Kelvin-Helmholtz and Rayleigh-Taylor Instabilities*. Imperial College London, London, http://wwwf.imperial.ac.uk/ ajm8/Hydrostab/kelvin.pdf, retrieved 2018-02-12.

[13] Per Nilsson *Particles-Following the stream or not*. LTH 2015.

[14] Isabel Maria Asenjo Gutierrez, *Two-Phase Fluid Flow Patterns under Microgravity Conditions*. Section of Aerothermodynamics, ESA, Noordwijk, 2002.

[15] Ronan Flanagan, *Operating Instructions, Spinning Test Rig*. NUMA Engineering Services Ltd, Ireland, 2017.

[16] L. Schiller, A. Naumann, *Uber die grundlegenden Berechnungen bei der Schwekraftaubereitung*. Zeitschrift des Vereines Deutscher Ingenieure, 77(12), 318-320. 1933

[17] Mário A.R.Talaia, *Terminal Velocity of a Bulbbel Rise in a Liquid Column* World Acedemy Science, Engineering Technology 28, 2007

A Videos

Most of the results for this report came from analyzing videos of the rotating LANG and BANNER tanks. The videos can be found online on the following webpages. Note that these videos are classified and are not available without the link:

A.1 LANG: Flow reaching Steady-State, seeded with Beige Particles

Link: https://youtu.be/GLyhbGTg2Sc//
Showing the the velocity vectors for the surface of the water for LANG. The velocity vectors are derived from tracking beige seeding particles on the water surface.

A.2 BANNER: Oscillations

Link: https://youtu.be/FYpzcbHTAss//
Showing videos of the electrolysis filmed from underneath the tank, camera rotating with the tank. The video is a compilation of different rotational speeds and visualizes the difference in stability and on-set oscillations present at certain rotational speeds.

A.3 BANNER: Flow Reaching Steady State, Seeded with Hydrogen Bubbles

Link: https://youtu.be/ldmVh3D5A2M//
Showing the flow reaching steady state for a closed tank rotating at 200 RPM. The fluid is first rotating slower than the cylinder wall but catches up in the end of the video. The video starts at 120 seconds after the start of spinning.

A.4 BANNER: Development of parabolic water surface in rotating fluid-filled cylinder

Link: https://youtu.be/mZAq9Lr5jRU//
Showing the water surface parabola forming as a open tank is rotated at 90 RPM, being half-filled with water. The surface is seeded with sunflower seeds that visualize the lowest point of the parabola.

B Bubbles

The flow is seeded with hydrogen bubbles created via electrolysis. A theoretical study is performed on the trajectory of a hydrogen bubble suspended in water. The bubble starts from the bottom a cylindrical tank at a distance to the axis of rotation. Different aspects of the trajectory is evaluated. Matlab will be used to calculate the different parameters of the bubble.

B.1 Coriolis Effect

The bubble will be subjected to a centripetal force pushing the bubble towards the axis of rotation, due to the higher density of water. It will at the same time be subjected to Coriolis acceleration as the bubble travels inwards. The centripetal acceleration is given by:

$$a_{cent} = \frac{u_\theta^2}{r} = (4 * 2 * \pi)^2 * 0.15 = 95 m/s^2 \tag{23}$$

Where u_θ is the azimuthal velocity and the a_{cent} is directed inwards in radial direction. The buoyant force on the bubble is given by:

$$F_{net} = \rho_{water} V_{bubble} * a_{cent} \tag{24}$$

Using equation 24, it can be seen that the bubble accelerate to $u = u_\infty = 0.07$ almost immediately. Therefore the radial velocity is set to 0.07 m/s, and the bubble is assumed to only accelerate due to Coriolis forces. The bubble is also assumed to not have negligible mass.

The Coriolis acceleration is given by:

$$\boldsymbol{a_{coriolis} = -2\Omega \times U} \tag{25}$$

Where the bold notation represent vectors and $\times$ is the cross product. The trajectory is plotted in polar coordinates (two-dimensional) and the movement in the upwards direction is assumed to not affect the trajectory of the bubble. The Rossby number gives the ratio of the inertial forces to the Coriolis forces. The Rossby number is given by:

$$Ro = \frac{U}{\Omega L} \tag{26}$$

Where U is the velocity of the bubble in reference to the spinning coordinate system, Ω is the rotational speed and L is the reference length which is the distance to center in this case. The planned rotational speed is $\Omega = 4 * \pi * 2$, the velocity in radial direction towards the axis is set to the terminal velocity of 0.07 m/s, and the radius is choses to 0.11 m, which gives a Rossby number of 0.025. A low Rossby number indicates that the inertial forces are not dominant. As an example, a trajectory for a rotational speed which gives Rossby number of on is also plotted:

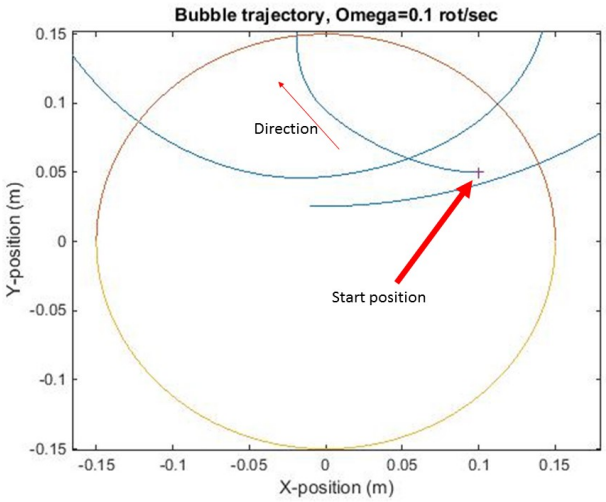

Figure 32: Theoretical trajectory of a bubble at relatively slow rotational speed

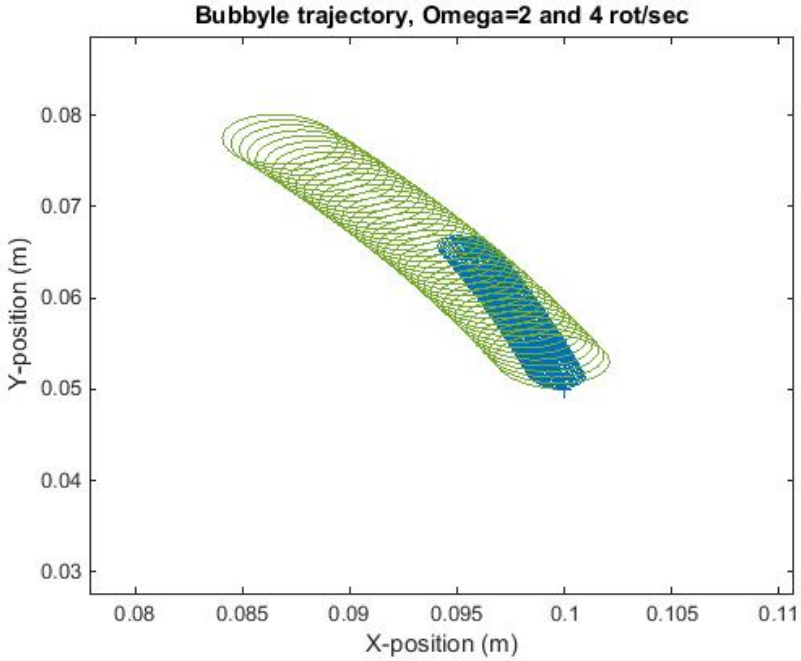

Figure 33: Trajectory when the bubble is dominated by Coriolis force

The trajectory is simulated for 10 seconds and the yellow line represents the wall of the cylinder. It can be seen that for low Rossby number the bubble should hit the wall, as for high Rossby numbers the bubble will rotate in small circles and move in a slow circular path around the cylinder.
If however the Coriolis forces are negligible, the bubble will only accelerate in inwards radial direction due to the centripetal force. This can be seen in experiments conducted by NASA, in this video https://www.youtube.com/watch?v=BxyfiBGCwhQ. Assuming that the bubble reaches terminal velocity in radial direction and maintaining constant, terminal velocity towards the center, the bubble will have the following trajectory, in a non-rotating coordinate system:

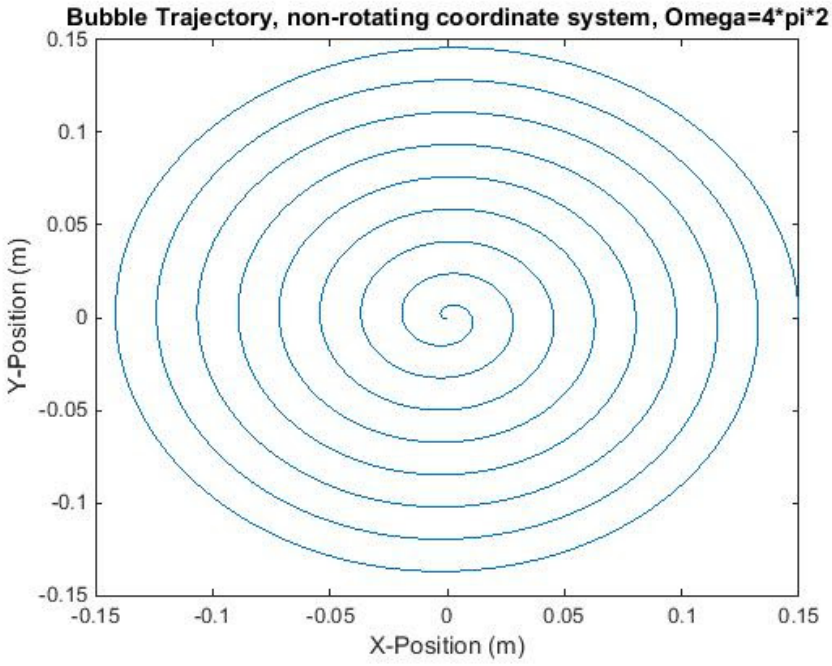

Figure 34: Theoretical trajectory of the bubble, assuming the bubble is not affected by the coriolis force

In the coordinate system of the spinning tank, the bubble will go in a straight line towards the axis of rotation.

B.2 Results from Preparatory bubble study

Before the electrolysis electronics were implemented in the experimental setup the bubbles were tested in LANG. Several test were made and compared with theoretical data.

B.2.1 Amount of bubbles created

A study was made on how the distance the wires would affect the number of bubbles created the result is shown in figure 35. It shows that the distance does primarily affect the number of bubbles created. The test was conducted in the order of the smallest distance first and largest distance last. What was noted was that the amount of bubbles seemed to increase the longer the current was ran through the water-sodium bicarbonate solution. Therefore, on this scale, it was determined that the distance would not be of importance for the experiments.

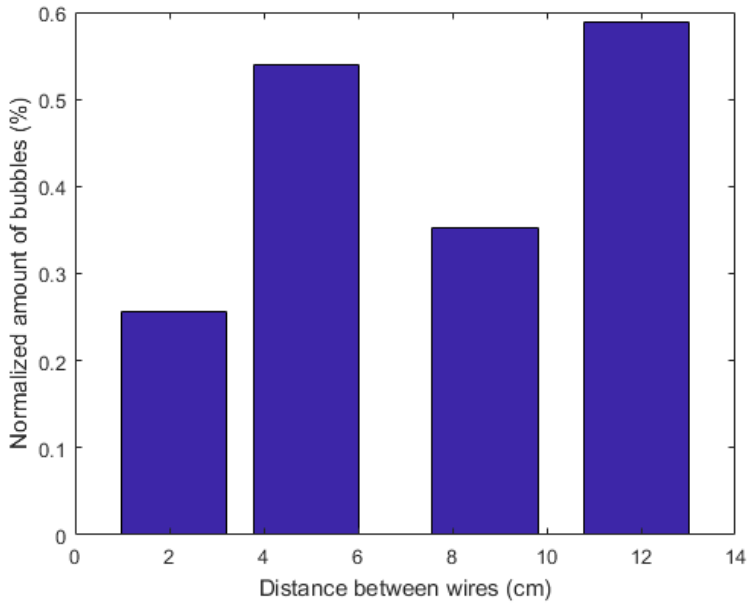

Figure 35: Amount of an experimental area covered by bubbles for different distances between the electrolysis wires

B.2.2 Velocities

There were two distinct types of bubbles created by the electrolysis. One were larger bubbles rising fast to the top of the tank. The other were slower rising bubbles which diffused into the water instead of rising to the top. The reason for some bubbles being fast and some being slower is believed to be due to adhesion of the hydrogen bubbles to the wire at certain points. The adhesion ensures that the bubbles are attached to wire for a longer time and can agglomerate more hydrogen gas. This makes them larger, which in turn gives them a larger buoyancy force. This makes them rise to the top. Since large bubbles were not of interest only one measurement was made on these bubbles that showed a velocity of 0.05 m/s.

The smaller bubbles do not have a large buoyancy force, which makes them stay in the middle of the tank, since they cannot overcome the force of the viscous forces in the water with the buoyancy force created by the lighter hydrogen compared to water. These bubbles are more valuable in the experiments since they stay longer at the same height and can be analyzed using PIV*.

The bubbles seem to generate their own flow field as the rise from the wire, see figure 36 and 37. The formation of the flow field is similar to a Rayleigh Taylor instability. This will affect the

results of the PIV*.

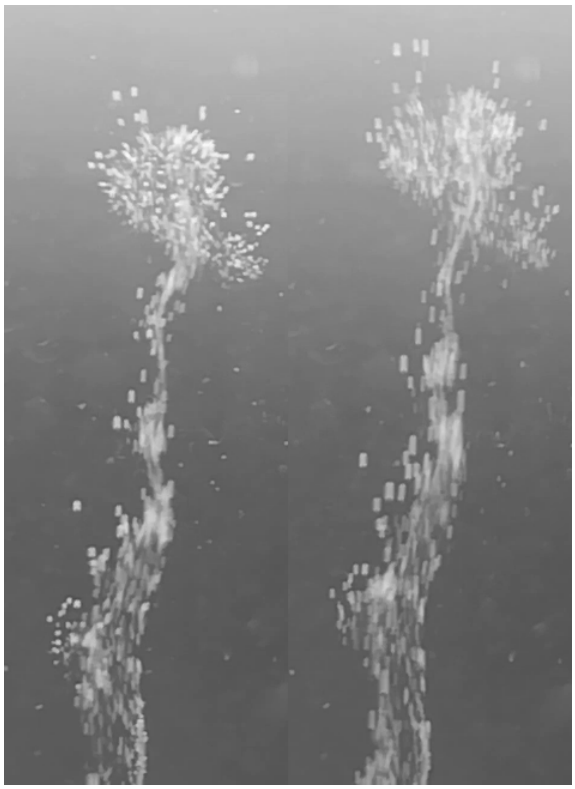

Figure 36: Two consecutive pictures of the bubbles from the side

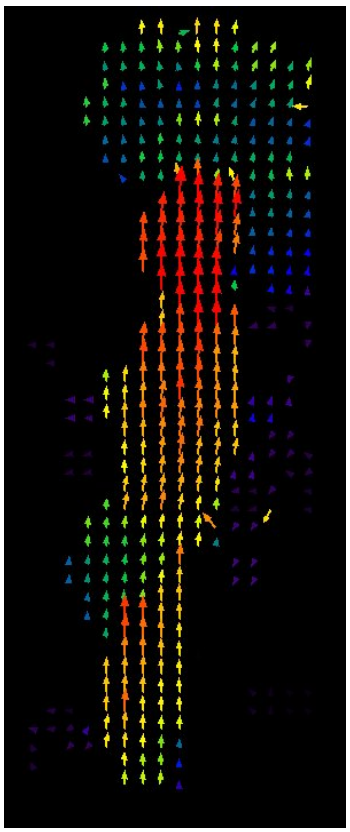

Figure 37: PIV* for the pictures seen in figure 36

B.2.3 Tracking the bubble trajectory

The small bubbles seem to accelerate straight inwards and not be affected by the Coriolis force, see figure 38. The image shows the bubbles velocity field for 200 RPM at steady sate. If the bubbles were affected by the Coriolis force the velocity field would be more chaotic, instead it now shows the bubbles going straight to the middle. The large bubbles however are affected by the Coriolis force, seen in figure 39. The bubble show a similar trajectory as seen in figure 33. Since these large bubbles rise so fast, they are not considered in the test, which means the test do not need to account for the Coriolis force.

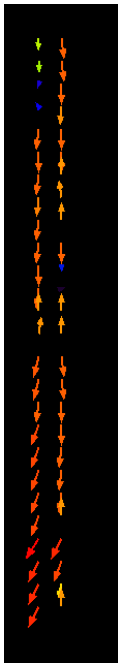

Figure 38: Velocity field around the cathode for steady state flow for 200RPM, with the middle being at the bottom of the image.

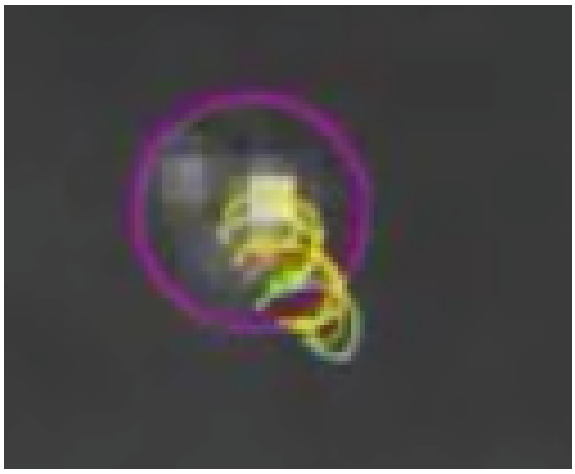

Figure 39: Trajectory for a larger bubble

B.3 Stokes Number

The Stokes number gives an indication on how well the seeding particles follows the flow. The definition of the Stokes number can vary in literature, in this report the same definition as used by Nilsson [2015] is going to be used:

$$St = \tau_p/\tau_f \tag{27}$$

The drag coefficient was given by 16:

$$c_d = \frac{24}{Re} * (1 + 0.15 * Re^{0.678}) \tag{28}$$

Where τ_p is the response time for the particle and τ_f is the response time for the fluid. The drag coefficient is going to be calculate in the same way as in equation 28. The density of water is given to $rho_f = 1000kg/m^3$, the density of hydrogen in gas form is $\rho_p = 89kg/m^3$, the velocity of the particle is 0.05 m/s.

The time scale for the particle is given by:

$$\tau_p = \frac{(u_f - u_p)}{\frac{du_p}{dt}} \tag{29}$$

$$\frac{du_p}{dt} = \frac{c_d * \pi * r^2 * \rho_f \frac{(u_f - u_p)^2}{2}}{\rho_p * \frac{4}{3}\pi * r^3} \leftarrow \tau_p = \frac{2\rho_p r^2}{9\rho_f \nu} * \frac{1}{1 + 0.15Re^{0.687}} \tag{30}$$

The response time for the fluid is given by:

$$\tau_f = \frac{l}{u_f} \tag{31}$$

For a rotational speed of $\Omega = 2\pi$, the Stokes number is 0.01. This indicates that the particle response time will always be small compared to the fluid response time. This is intuitive since the particle is light relative to the water and relatively small for a seeding particle.

C Results of Parabola tracking in BANNER

C.1 Tracking lowest point on parabola

The pictures below show the derivative of the smoothed function of the coordinate of the lowest point of the parabola given as function of time. When the value of 0.001 was chosen as a reference value for when the fluid had reached steady state. If the derivative did not reach this value, a the plot of the smoothed function was analyzed and an estimation of the steady state was made. Each plot-line represents one test. Not all tests were used in the final results since some of the derivatives do not behave physically, see figure 47. The figures show a discontinuities and change in a way that does not seem intuitive. This is caused by the way the function is smoothed to make sure the derivative approximates zero when steady state is reached by the fluid.

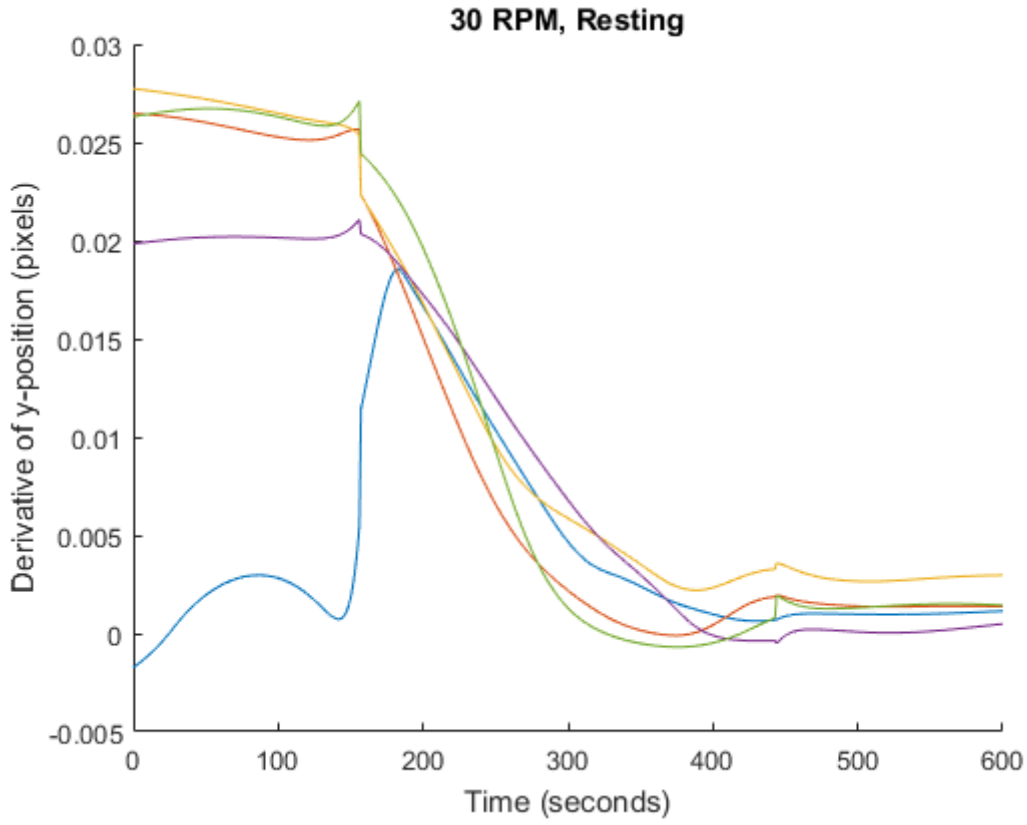

Figure 40: The derivatives of the y-position of the lowest point of the parabola as a function of time, 30 RPM, Resting fluid

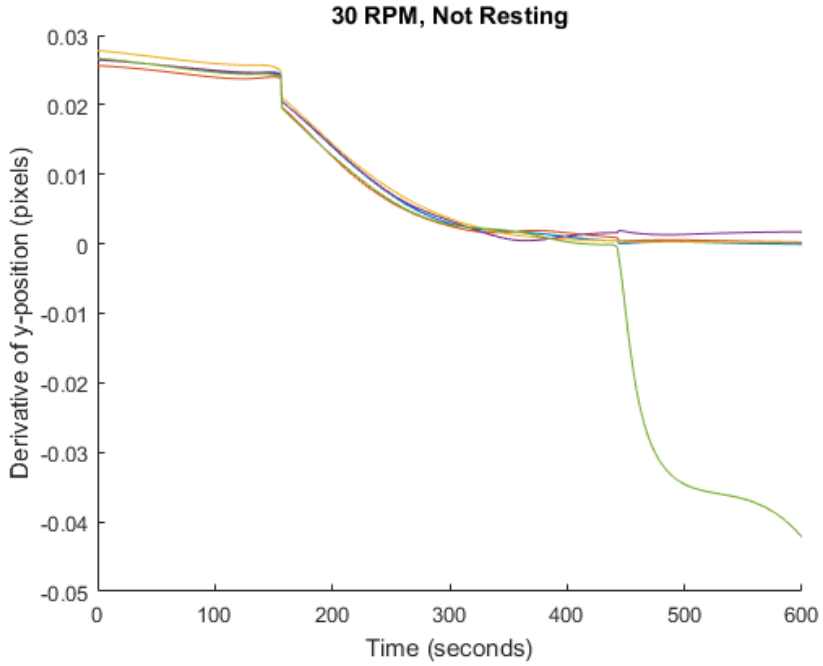

Figure 41: The derivatives of the y-position of the lowest point of the parabola as a function of time, 30 RPM, Non-Resting fluid

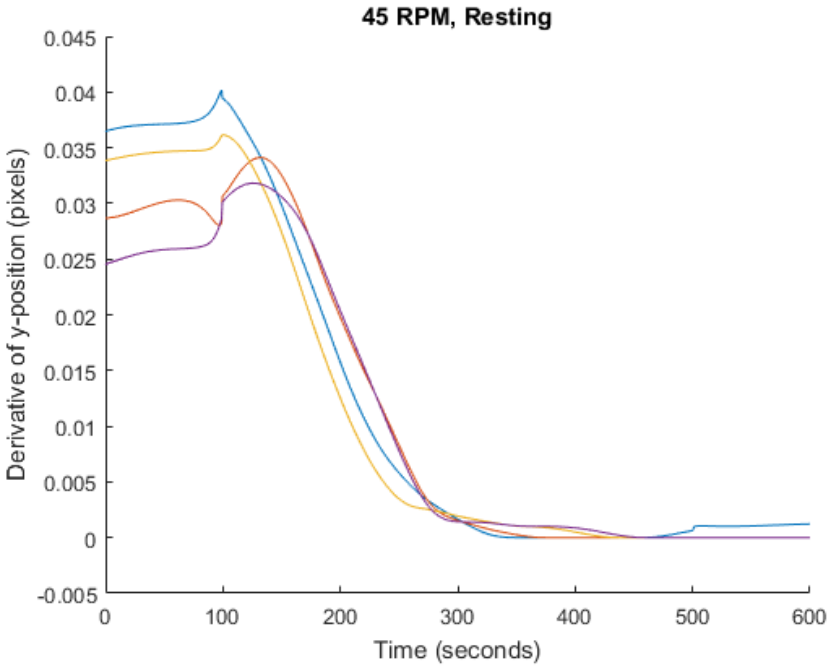

Figure 42: The derivatives of the y-position of the lowest point of the parabola as a function of time, 45 RPM, Resting fluid

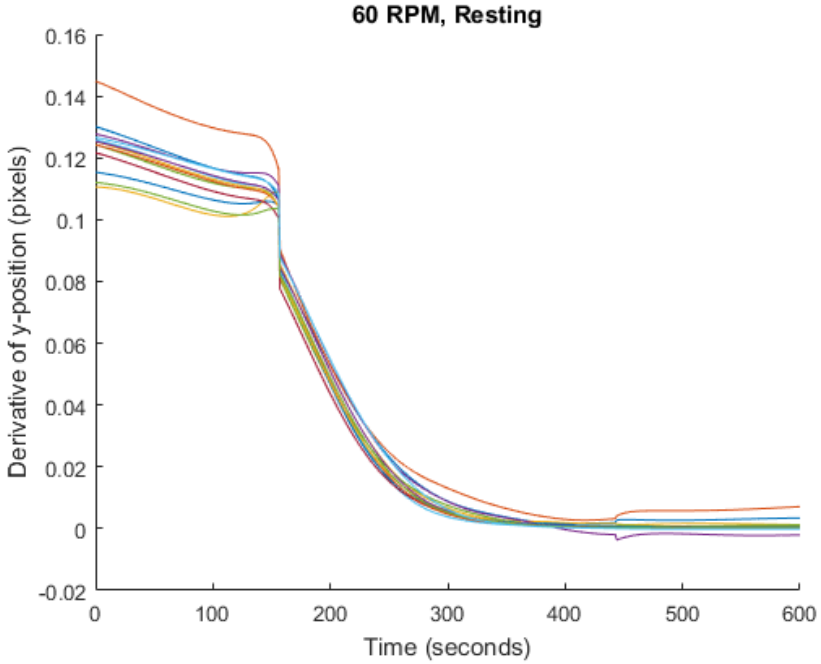

Figure 43: The derivatives of the y-position of the lowest point of the parabola as a function of time, 60 RPM, Resting fluid

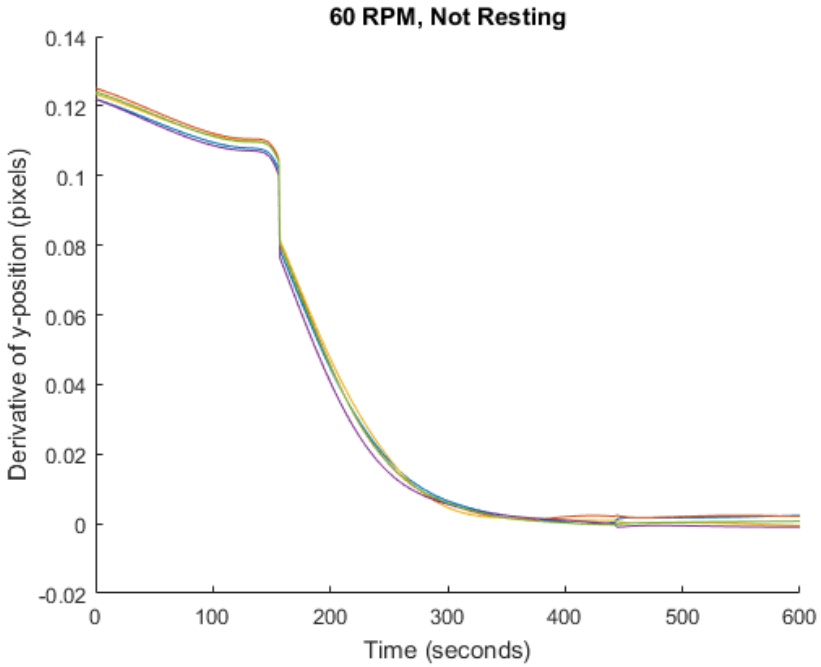

Figure 44: The derivatives of the y-position of the lowest point of the parabola as a function of time, 60 RPM, Non-Resting fluid

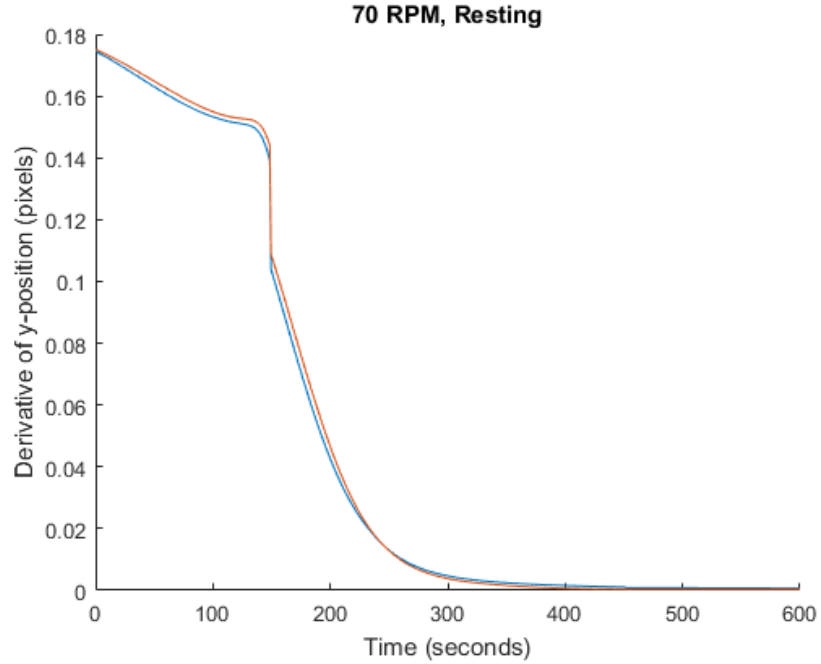

Figure 45: The derivatives of the y-position of the lowest point of the parabola as a function of time, 70 RPM, Resting fluid

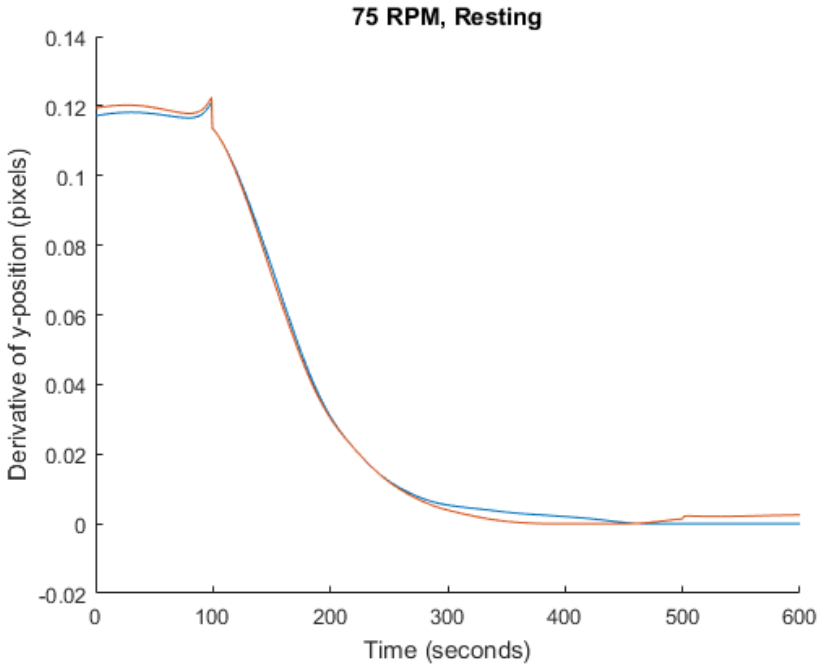

Figure 46: The derivatives of the y-position of the lowest point of the parabola as a function of time, 75 RPM, Resting fluid

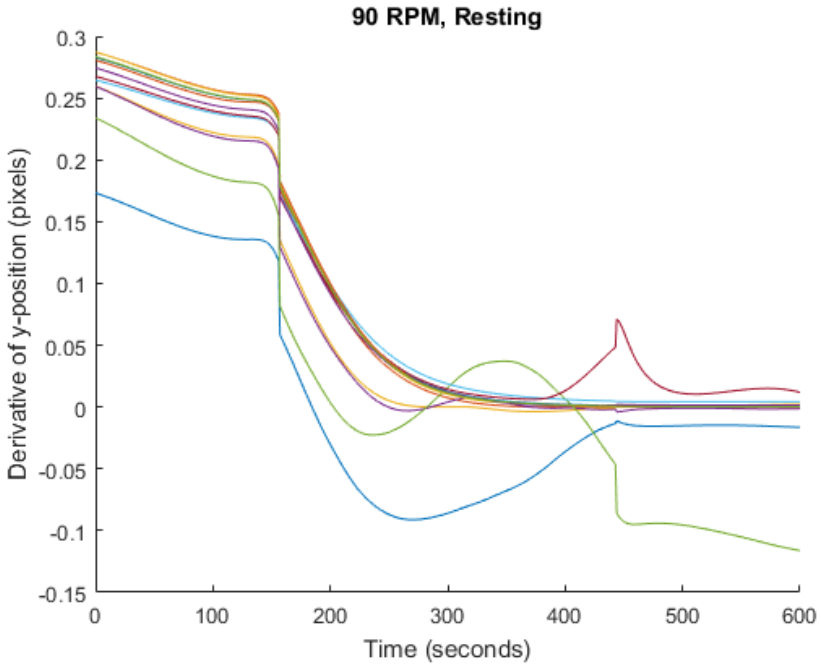

Figure 47: The derivatives of the y-position of the lowest point of the parabola as a function of time, 90 RPM, Resting fluid

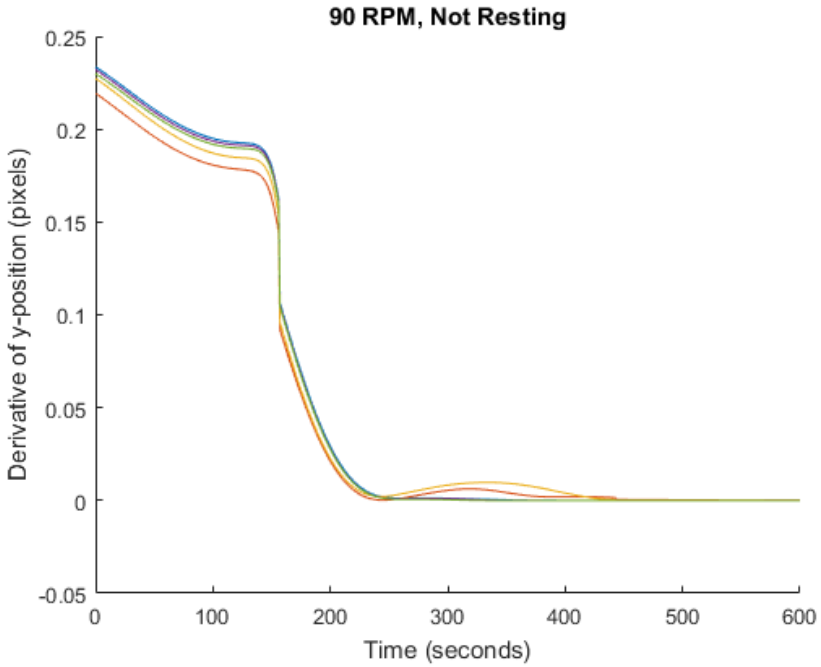

Figure 48: The derivatives of the y-position of the lowest point of the parabola as a function of time, 90 RPM, Non-Resting fluid

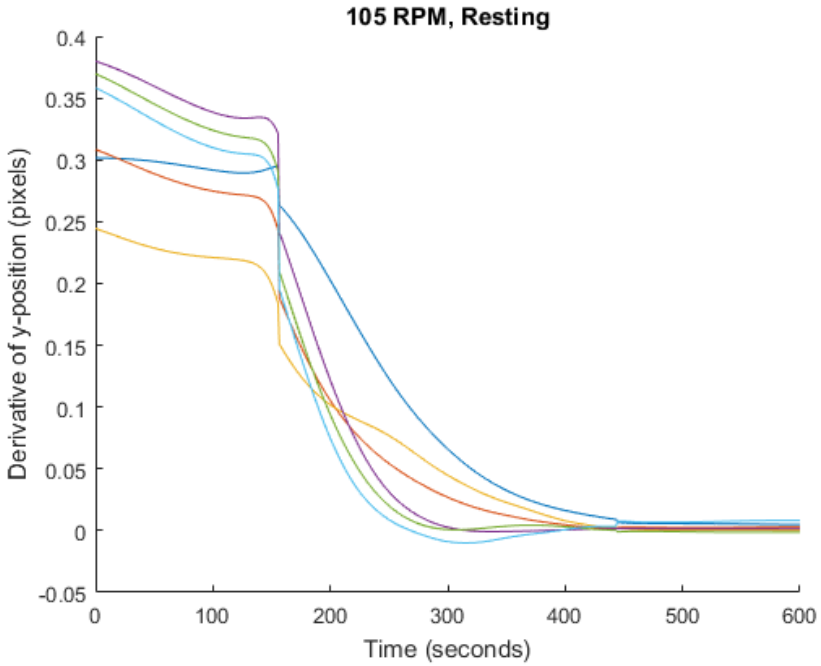

Figure 49: The derivatives of the y-position of the lowest point of the parabola as a function of time, 105 RPM, Resting fluid

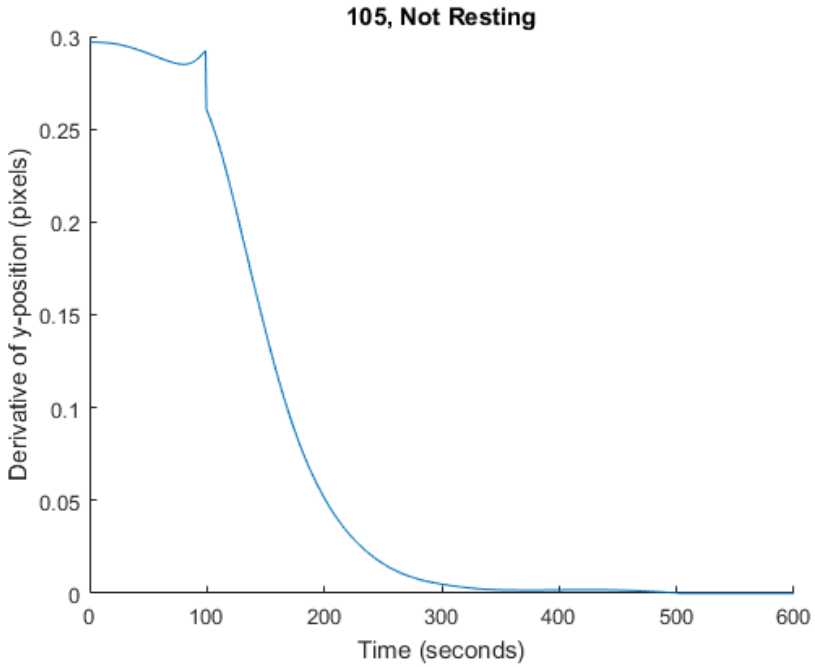

Figure 50: The derivatives of the y-position of the lowest point of the parabola as a function of time, 105 RPM, Non-Resting fluid

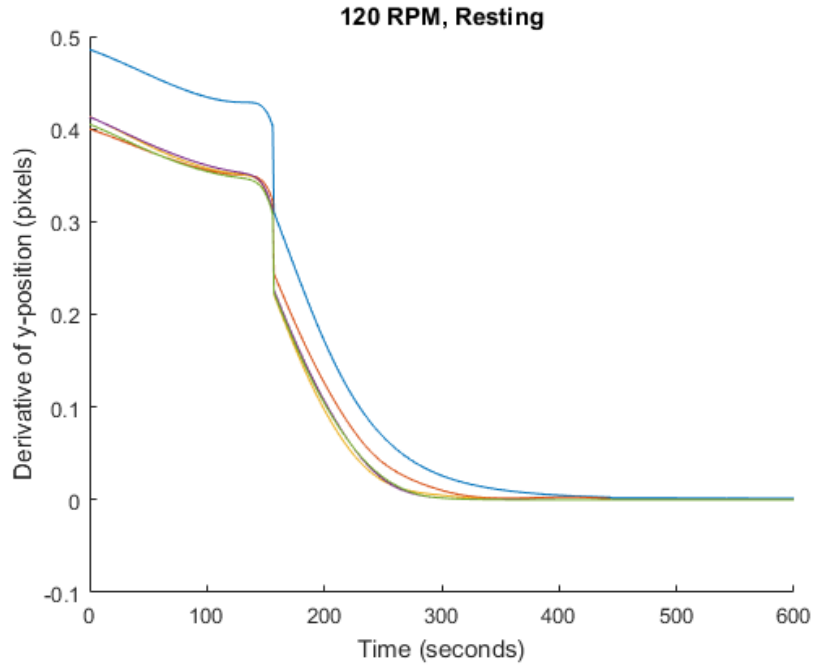

Figure 51: The derivatives of the y-position of the lowest point of the parabola as a function of time, 120 RPM, Resting fluid

C.2 Using PIV* to determine steady state

The method of tracking the lowest point of the parabola was verified using the method of PIV* with hydrogen bubbles created by electrolysis. The velocity in azimuthal direction was measured (θ-direction as seen in figure 1). The velocity was averaged over an area and normalized by the same area. Since the camera is spinning with the tank, the velocity profile will not be linear, but instead a zero-velocity profile. The fluid is said to reach steady state the first time the Savitzky-

Golay smoothed function reaches zero. Some of the measurements are offset by some value, which is due to the experimental method not being perfect.

For the measurement of the open tank spinning at 90 RPM, the bubbles were in constant oscillation, which ensured that the velocity profile did not reach steady state. All PIV*-measurements were backed up with visual quantification of the flow. When the fluid reaches steady state, the bubbles do not travel in azimuthal direction, so the steady state time for the measurement of the 90 RPM was determined visually, see figure 54, figure 56 and figure 57.

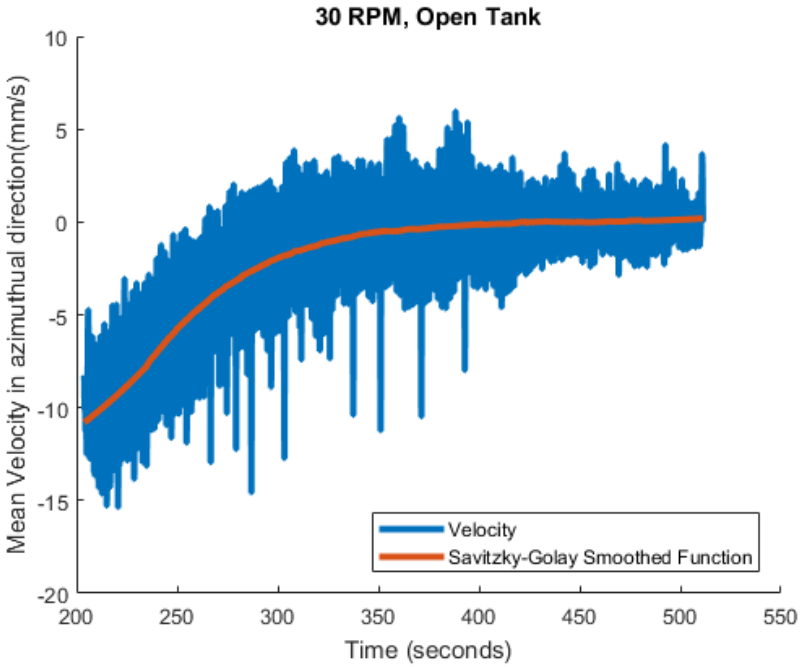

Figure 52: The mean azimuthal velocity. Steady state reached at 420 seconds.

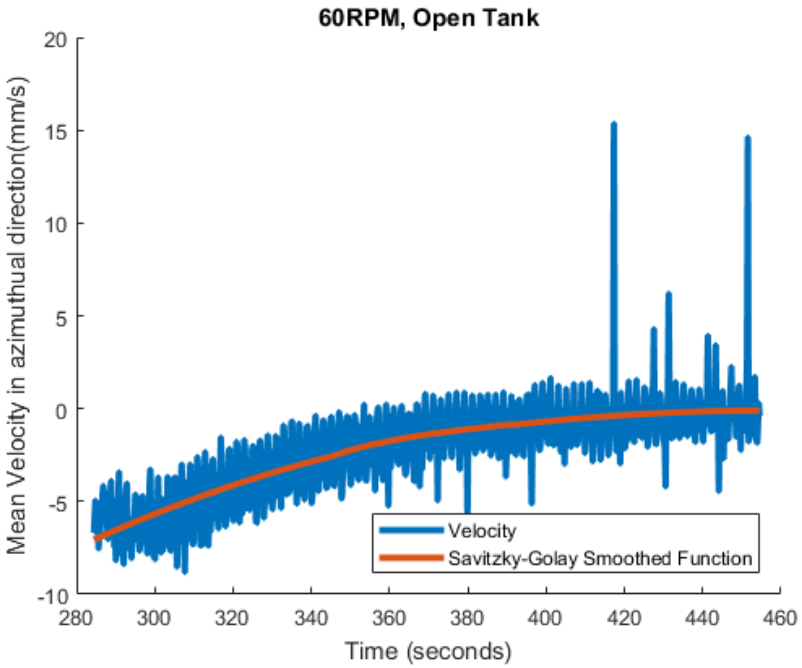

Figure 53: The mean azimuthal velocity. Steady state reached at 420 seconds.

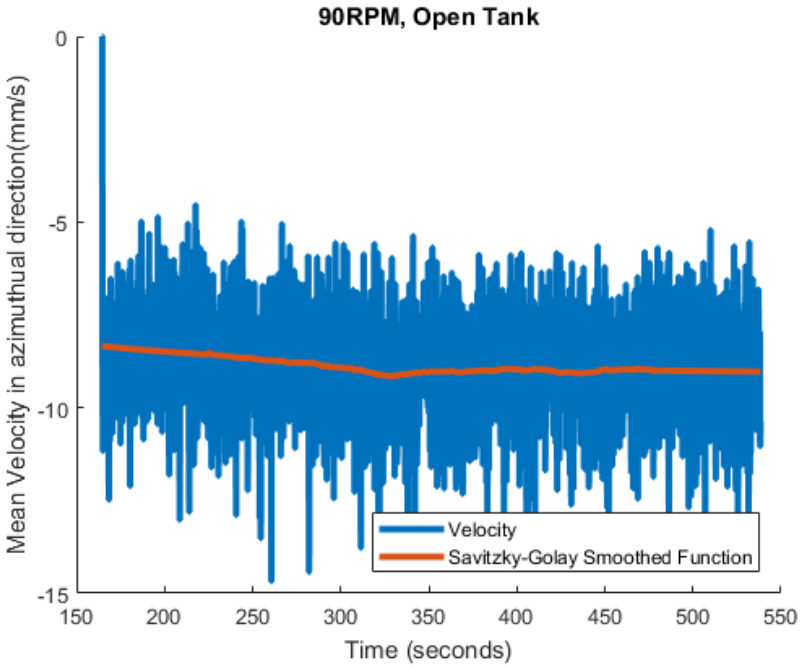

Figure 54: The mean azimuthal velocity. Steady state time can not be determined

In figure 55 the Fourier transform for the velocity measurement as a function of time for BANNER at 90 RPM can be found. The dominant frequency is 1.5 Hz, corresponding to the RPM. This indicates that something happens every time BANNER rotates. The flow could be speeding up or slowing down once every rotation.

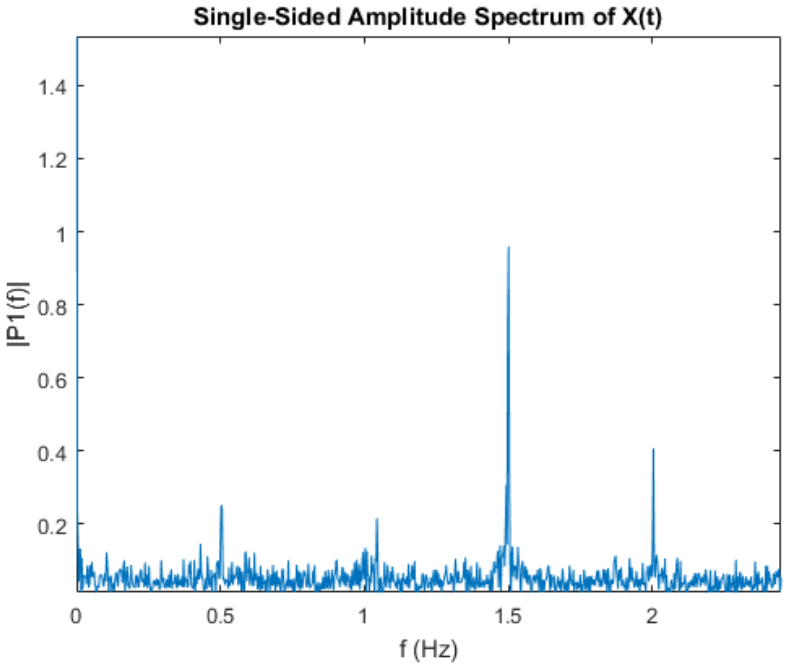

Figure 55: The Fourier transform of the velocity in BANNER Half-filled at 90RPM.

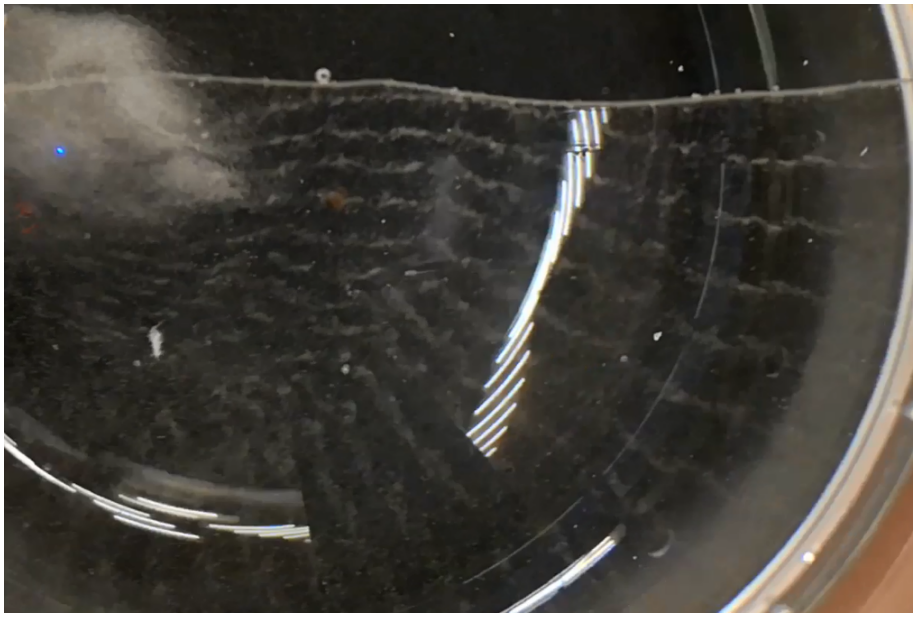

Figure 56: Showing BANNER from below with bubble formation after 280 seconds.

Figure 57: Showing BANNER from below and bubble formation at 370 seconds. Closest point to steady-state

D Results for BANNER Fully-filled

The flow was analyzed the same was as for BANNER Half-filled using hydrogen bubbles as seeding for a PIV*-method. The velocity was averaged over an area where the particles had high constrast against the backgroung and normalized with the same area. The camera is mounted in the same frame as the cylinder which means that a mean velocity that is not equal to zero represents the fluid moving slower than the rotating cylinder. The camera was not mounted the same way every time which causes some of the graphs to have a inverse y-axis. This is explained in the caption under each graph. The criterion for steady state is either when the velocity reaches zero or the derivative of the velocity reaches a value close to zero. When the velocity does not reach zero it is believed to be due to error in the measuring method.

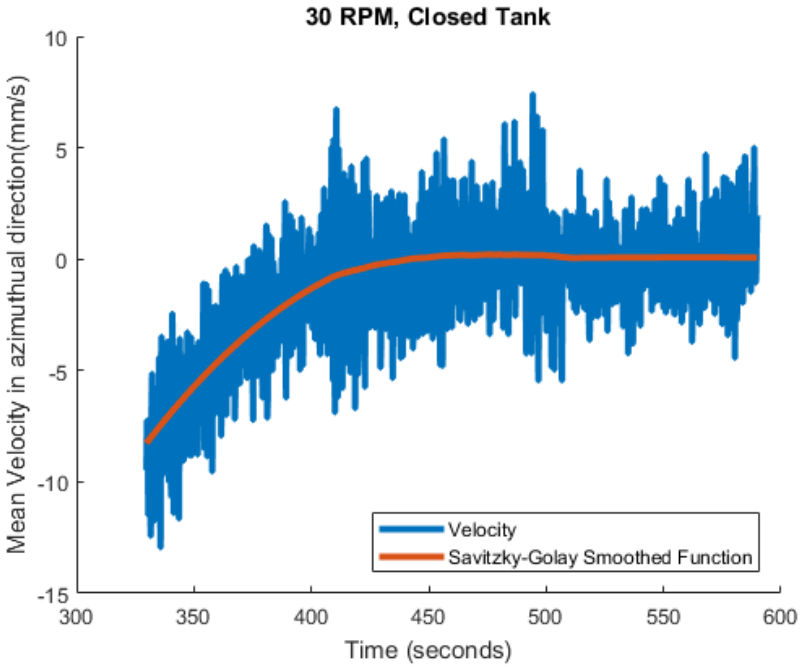

Figure 58: The mean azimuthal velocity for BANNER Fully-filled at 30 RPM. Steady state reached at 442 seconds.

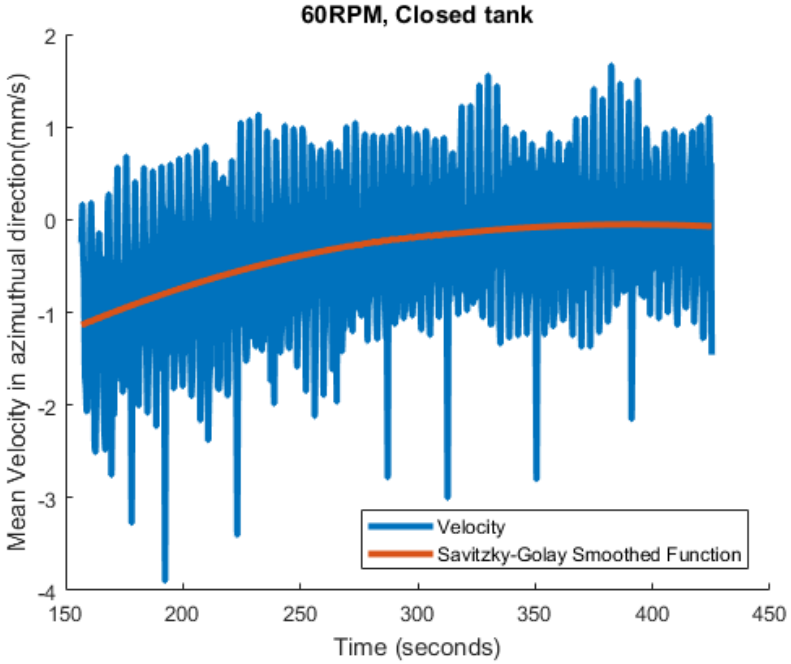

Figure 59: The mean azimuthal velocity for BANNER Fully-filled at 60 RPM, first test. Steady state reached at 340 seconds.

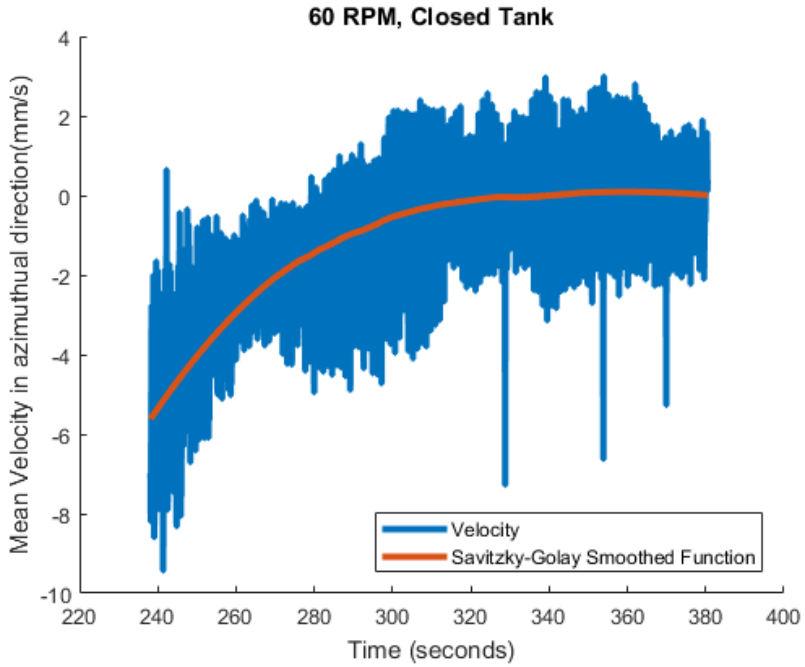

Figure 60: The mean azimuthal velocity for BANNER Fully-filled at 60 RPM, second test. Steady state reached at 338 seconds.

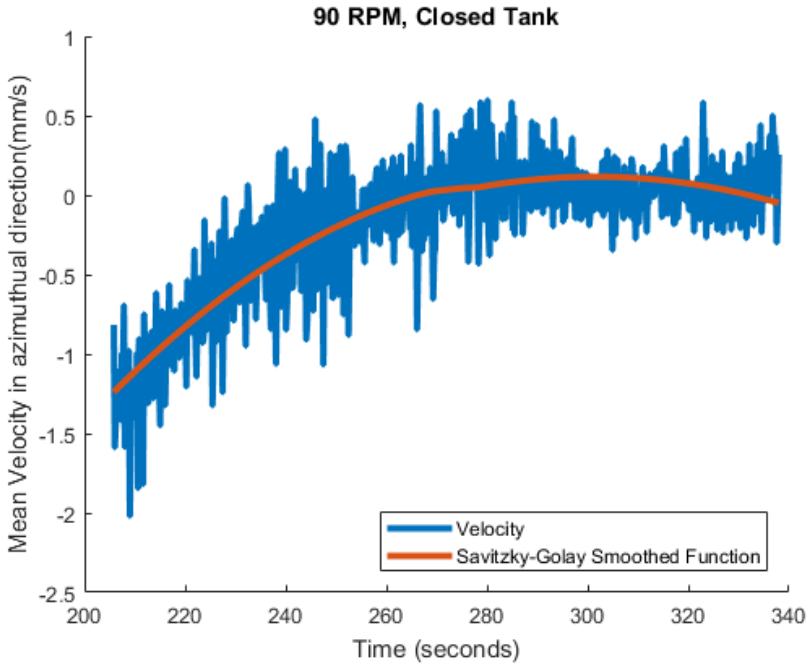

Figure 61: The mean azimuthal velocity for BANNER Fully-filled at 90 RPM. Steady state reached at 290 seconds.

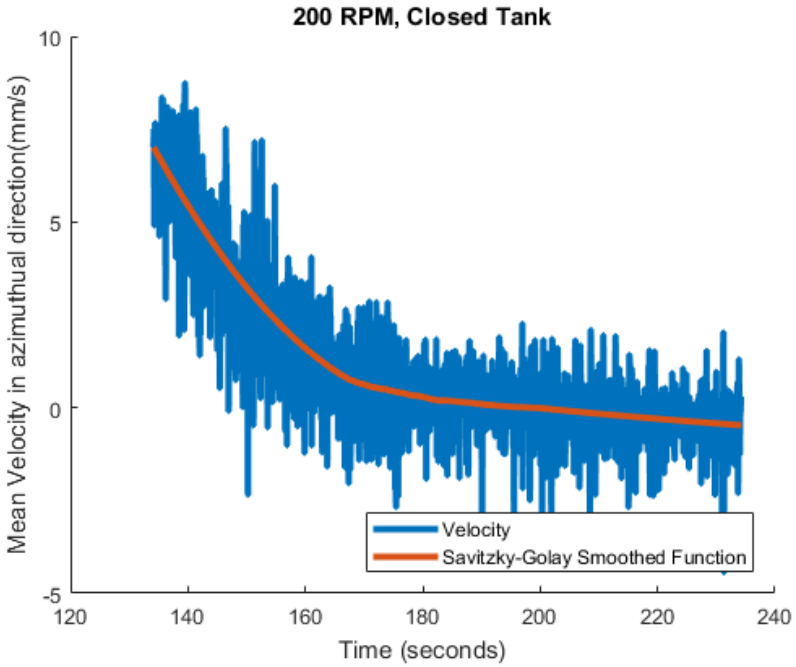

Figure 62: The mean azimuthal velocity for BANNER Fully-filled tank at 200 RPM, test 1. Steady state reached at 198 seconds.

The test for 200 RPM were conducted the same way as the second test at 60 RPM, were the θ-direction is called the x-direction. Note that the camera is mounted in the opposite direction in the first test for 200 RPM, meaning that the azimuthal velocity goes towards zero from positive values instead of negative values. This means that positive x-values are representing a slower velocity than the wall velocity of the cylinder. The values of the velocities in the experimental test for 200 RPM are normalized with the wall speed of the cylinder.

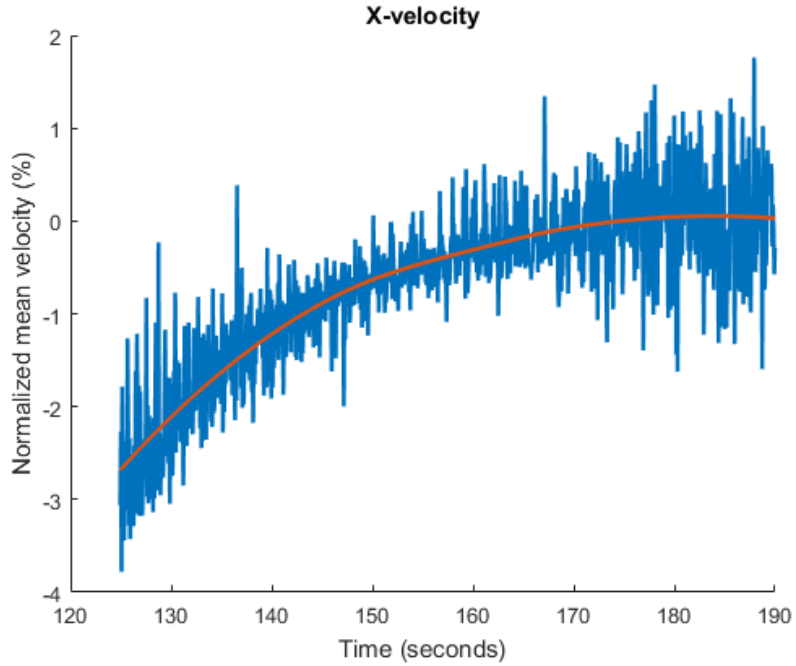

Figure 63: The mean azimuthal velocity for BANNER Fully-filled at 200 RPM, test 1. Steady state reached at 180 seconds.

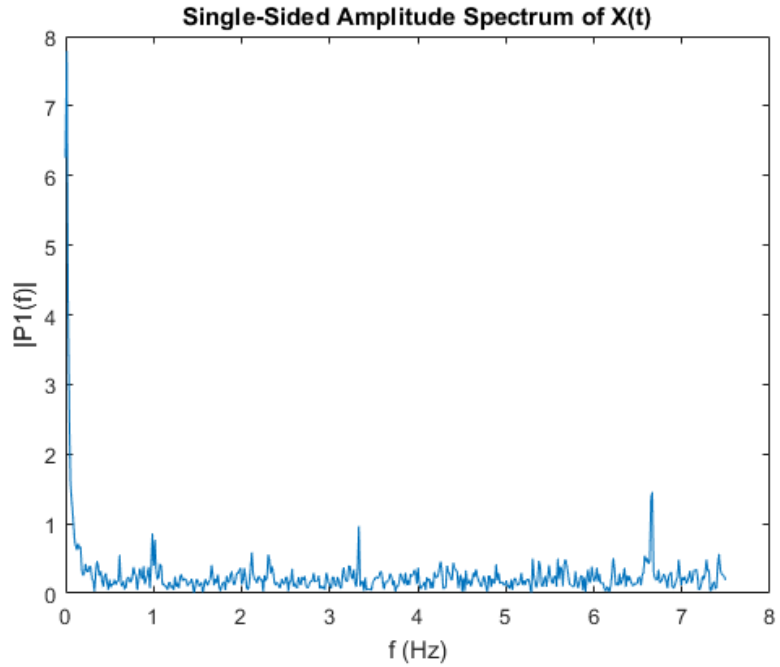

Figure 64: The Fourier transform for the velocity measurements for BANNER Fully-filled at 200 RPM. Showing no dominant frequencies.

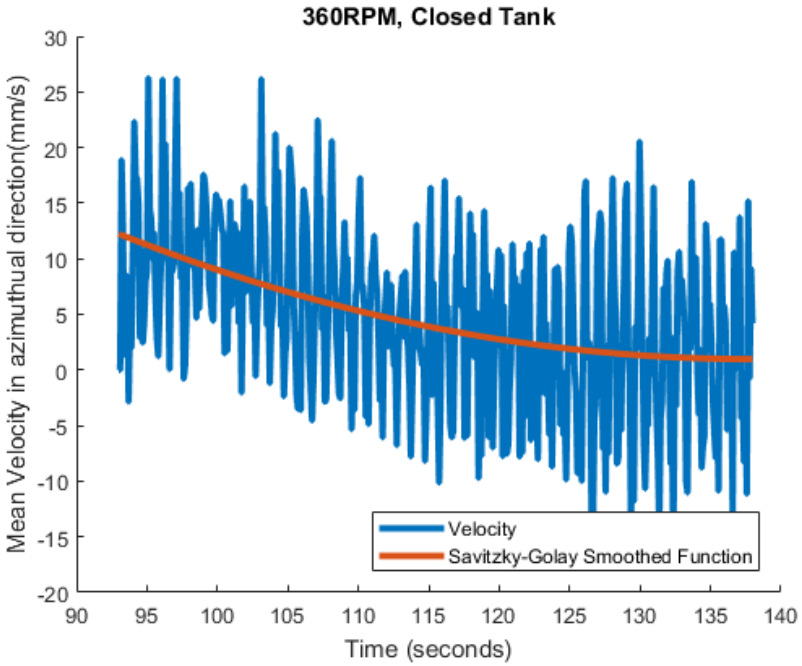

Figure 65: The mean azimuthal velocity for BANNER Fully-filled at 360 RPM. Steady state reached at 130 seconds.

The measurement of 30 RPM is the limit of what the test-setup could handle. The test-standing was shaking due to the relatively large stresses caused by the high rotational speed. It should be noted that it is expected that the rotations per seconds should show up as a dominant frequency in the Fourier transform, but the sampling frequency is to low according to the Nyquist criterion to detect the frequency.

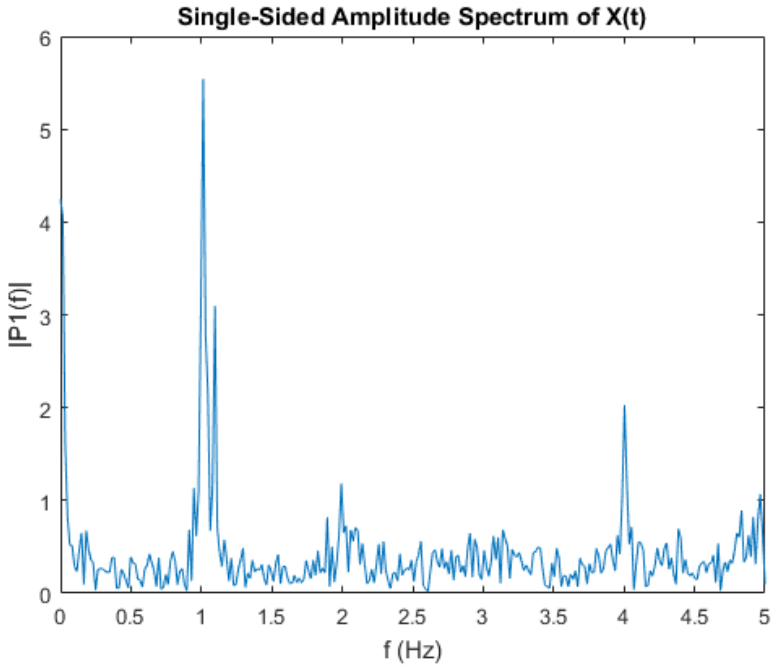

Figure 66: The Fourier transform for the velocity measurements for BANNER Fully-filled at 360 RPM. Showing dominant frequency at 1 Hz. Sampling frequency is 10 Hz.

E Theory on spin-up times from rest of a fluid-filled cylinder

Munk [2] did a compilation of different theoretical works on the spin-up from rest of a completely fluid-filled cylinder. The works are based on Wedemeyer, Venezian, Weidman and Greenspan. The theory is based on a case were the cylinder is impulsively set to the constant, final rotational speed.

The non-linearities are divided in different ranges, one for $Ro < 0.5$ and one for $Ro > 0.5$. If $Ro < 0.5$ the non-linear processes are non-dominant and do not diverge significantly from linear theory. When $Ro > 0.5$ a new, non-linear phenomenon is created. The inner part of the Stewardson layer is detached from the vertical walls and propagates towards the axis of rotation.

The Wedemeyer model uses the Navier-Stokes equations for incompressible, constant-viscosity, no-body forces and axis-symmetric fluid in cylindrical coordinates, see figure 1 for coordinates and 2 for orientation of velocity vectors.

$$\frac{\partial V}{\partial t} + U\left(\frac{\partial V}{\partial r} + \frac{V}{r}\right) + W\frac{\partial V}{\partial z} = \nu\left[\frac{\partial^2 V}{\partial r^2} + \frac{\partial}{\partial r}\left(\frac{V}{r}\right) + \frac{\partial^2 V}{\partial z^2}\right] \tag{32}$$

$$\frac{\partial U}{\partial t} + U\frac{\partial U}{\partial r} + W\frac{\partial U}{\partial z} - \frac{V^2}{r} + \frac{1}{\rho}\frac{\partial P}{\partial r} = \nu\left[\frac{\partial^2 U}{\partial r^2} + \frac{\partial}{\partial r}\left(\frac{U}{r}\right) + \frac{\partial^2 U}{\partial z^2}\right] \tag{33}$$

$$\frac{\partial W}{\partial t} + U\frac{\partial w}{\partial r} + W\frac{\partial w}{\partial z} + \frac{1}{\rho}\frac{\partial P}{\partial z} = \nu\left[\frac{\partial^2 W}{\partial r^2} + \frac{1}{r}\frac{\partial W}{\partial r} + \frac{\partial^2 W}{\partial z^2}\right] \tag{34}$$

And the continuity equation:

$$\frac{\partial (rU)}{\partial r} + \frac{\partial (rW)}{\partial z} = 0 \tag{35}$$

The flow assumed to not be affected by body-forces, meaning that gravity is not taken into account. The density is assumed to be constant. The boundary conditions are given by:

$$U = W = 0, V(z = 0) = V(z = h) = V(r = R) = r\Omega \tag{36}$$

This assumes the walls of the cylinder have a non-slip boundary condition. Munk [2] points out that having an infinity long cylinder would reduce equation 32 to a linear differential equation only dependent on r and t. The non-linearity of the set of differential equations finite length of the cylinder inducing secondary flow, giving non-zero values for the velocities in z- and r-direction.

Wedemeyers analytical derivation assumes that the secondary flow is slow at the core. This means all time and spatial dependencies for the radial veolcity component in the core flow, denoted by u_0 are neglected. The index of "0" indicates core flow. Equation 33 becomes:

$$\frac{1}{\rho}\frac{\partial P_0}{\partial r} = \frac{V_0^2}{r} \tag{37}$$

In the core flow, V_0 is independent of z. Since u is not longer part of the equation, equation 32 becomes:

$$\nu\left[\frac{\partial V_0}{\partial t} + U_0\frac{\partial V_0}{\partial r} - \frac{VU_0}{r}\right] = \frac{\partial}{\partial r}\left(\frac{1}{r}\frac{\partial rV_0}{\partial r}\right) \tag{38}$$

Note that this equation needs to be solved for $V_0(r,t)$, which means that $U_0(r,t)$ needs to be solved first.

The boundary layer equations are given by:

$$U\frac{\partial U}{\partial r} + W\frac{\partial U}{\partial z} - \frac{V^2}{r} + \frac{V_0^2}{r} = V\frac{\partial^2 U}{\partial z^2} \tag{39}$$

$$U\frac{\partial U}{\partial r} + u\frac{U}{r} + w\frac{\partial V}{\partial z} = \nu\frac{\partial^2 V}{\partial z^2} \tag{40}$$

With the continuity equation the same as equation 35. The boundary conditions at $z = 0$ are given by:

$$V = r\Omega, U = 0, W = 0 \tag{41}$$

And the boundary conditions at $z = h$ are given by:

$$V = V_0(r,t), U = 0 \tag{42}$$

For the general v_0-distribution, when neither linearization nor the assumption of similarity in flow is applicable, the approximate solution can be attained using momentum-integral methods. The momentum-integral method does provide an exact shape of the velocity profile but it provides fairly in-accurate approximations of integral values. The equation for axis-symmetric radial mass-flow, assuming constant density in the boundary layer is given by:

$$M(r) = 2\pi\rho r\int_0^\delta U(r,z)dz \tag{43}$$

Where δ is the boundary layer thickness. When the radial mass-flow distribution has been determined- for a given distribution of $V_0(r)$- the radial velocity of the core can be found. Due to the fact that the total radial mass-flow needs to be be zero in the two boundary layers and the core-flow the following equation is obtained:

$$2\pi r\rho\left[2\int_0^\delta U(r,z)dz + hU_0(r)\right] = 0 \tag{44}$$

or:

$$-\frac{1}{2}hU_0(r) = \int_0^\delta U(r,z)dz \tag{45}$$

Equation 44 can be visualized using figure 67. The boundary layer flow for the vertical wall is not visualized since it is will become the core flow when the flow detaches from the wall. The dashed line shows the movement as the Ekman layer-flow reaches the vertical wall and how the vertical boundary layer (Stewardson Layer) forms the core flow (inviscid flow).

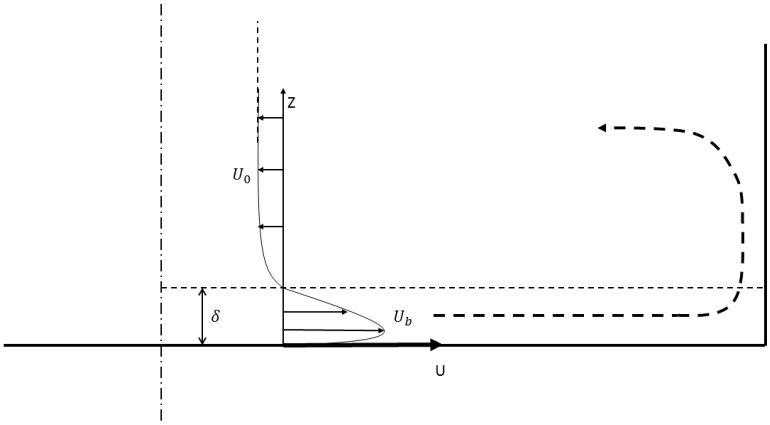

Figure 67: The equilibrium in volume-flow for the r-z plane caused by Ekman pumping.

This equation is solved by Wedemeyer referring to the work of Cochrans solutions for differential equations describing rotating disc flow as:

$$\int_0^\delta U(r,z)dz = 0.443\sqrt{\frac{\nu}{\Omega}}r\Omega \tag{46}$$

Using linear interpolation, the core flow can be implemented using:

$$\int_0^\delta u(r,z)dz = 0.443\sqrt{\frac{\nu}{\Omega}}(r\Omega - v_0) \tag{47}$$

The same equation is solved according to Greenspan and Ludweig:

$$-\frac{1}{2}hU_0(r) = \int_0^\delta U'dz = 0.5v_0'\sqrt{\frac{\nu}{\Omega}} \tag{48}$$

Where $v_0 = v_0 - r\Omega$. Equation 47 and 48 are the same with the only difference being the factor of 0.443 or 0.5. According to Sedney and Gerber, 0.5 gives better agreement with numerical simulations. Using the Reynolds number $Re = \frac{2a\Omega}{\nu}$ and implementing the parameter of k, equation 48 is rewritten as:

$$k = \frac{u_0}{v_0 - r\Omega} = 0.5 * \left(\frac{2a}{c}Re^{-1/2}\right) \tag{49}$$

This might seem counter intuitive, since it would seem the value would always be negative. This is not the case since the core-flow of u_0 is always negative until steady state where $u_0 = 0$. Examining equation 49 it is found that the term $v_0 - r\Omega$ can be regarded as a measurement on how close the fluid is to steady state rotation.The parameter k can be seen as the inverse residual velocity of the core flow (The difference between the core flow and the steady state solution) normalized with the radial core-flow, which would be the same as non-dimensional spin-up time, depending on the criterion for steady-state. The criterion is chosen in the v_0 term, as an example 99 % of the change of inertia would mean that $v_0 = 0.99 * r\Omega$. We now have a model for the spin-up time, using only physical parameters in the cylinder. Using the half-height of the cylinder, as done by Sedney and Gerber the following formula for the spin-up time is found:

$$t = \frac{1}{k * \Omega} = \frac{\frac{2c}{a}\sqrt{Re}}{\Omega} = \frac{2}{\sqrt{Ek} * \Omega} \tag{50}$$

Which is the same as found by Sedney and Gerber.

F Solving Navier-Stokes equations Numerically

To examine the affect of the secondary flows, the Navier-Stokes equations are solved for the one-dimensional, axis-symmetric, incompressible case. Only the velocity in the azimuthal direction is taken in cosideration and it is assumed that the velocity only changes over time in the radial direction. The Navier-Stokes equation in cylindrical coordinates simplifies to:

$$\frac{\partial V}{\partial t} = \nu \left[\frac{1}{r} \frac{\partial}{\partial r} \left(r \frac{\partial V}{\partial r} \right) \right] \tag{51}$$

The equation is a parabolic partial differential equation and can be solved numerically using forward differentiating scheme for the time and second order central differentiating scheme.